PIONEER RESEARCH IN

NATURAL SCIENCE AND

MATHEMATICS

PIONEER RESEARCH IN NATURAL SCIENCE AND MATHEMATICS

Editor
Assoc. Prof. Dr. HÜLYA ÇELİK

Pioneer Research in Natural Science and Mathematics
Editor: Assoc. Prof. Dr. HÜLYA ÇELİK

www.allsciencesacademy.com
allsciencesacademy@gmail.com

CONTENT

Complete (11,3)-Arcs Constructed from Menelaus Configurations in PG(2,5) via Secant-Based Analysis

Ayşe BAYAR[1]
Elif ALTINTAŞ KAHRİMAN [2]

1- Assist Prof. ; Bartın University, Department of Management Information System, Bartın University, Faculty of Economics and Administrative Sciences,. ealtintaskahriman@bartin.edu.tr ORCID No: 0000-0002-3454-0326
2- Prof. ; Eskişehir Osmangazi University, Department of Mathematics and Computer Sciences, Eskişehir Osmangazi University, Faculty of Science,. akorkmaz@ogu.edu.tr ORCID No: 0000-0002-2210-5423

ABSTRACT

This study investigates the construction and classification of complete *(11,3)*-arcs in the projective plane PG(2,5) that include a Menelaus configuration. A computational algorithm implemented in C# is used to identify and classify the points outside the Menelaus configuration based on their secant line interactions—specifically 0-secant, 1-secant, and 2-secant incidences. Thirteen such points are identified and grouped into three categories. Based on this categorization, two structured methods are developed for constructing complete *(11,3)*-arcs.

The first method focuses on a triangle formed by three Category 3 points, each with two 2-secant lines. By selecting one point from each of two different triangle sides and then adding three suitable Category 2 points, twelve distinct complete *(11,3)-arcs* are obtained. The second method begins by adding all Category 2 points not lying on the triangle's sides to the Menelaus configuration, forming an incomplete *(10,3)-arc*. Then, one of the six remaining Category 1 points is added to yield six more complete *(11,3)-arcs*. In total, eighteen distinct complete *(11,3)-arcs* containing a Menelaus configuration are constructed. This work contributes to the geometric and combinatorial understanding of arcs in finite projective planes and demonstrates how secant-based classifications can guide systematic arc construction in *PG(2,5)*. The results also highlight the computational power of algorithmic approaches in finite geometry.

Keywords – finite projective plane; (k,3)-arc; Menelaus configuration; secant lines

INTRODUCTION

Arcs hold significant importance in projective geometry and are widely utilized in combinatorics and related disciplines. A *k*-arc refers to a set *K* of *k* points ($k \geq 3$) in a finite projective plane π, with the condition that no three points lie on the same line. A special case of an arc, known as a hyperoval, consists of *(p + 2)* such points. The maximum possible value of *k* is attainable only when the order *p* of the projective plane π is even, in which case $k \geq p+2$. In existing literature, ovals are frequently studied, with Hirschfeld being one of the most commonly referenced authorities on the subject [1]. Extensive research has been conducted on arcs in projective planes, with particular emphasis on complete *(k,2)*-arcs that form complete quadrangles. Such configurations, as examined in [2, 3], give rise to Fano planes within the projective setting. In [4], the authors explore how Fano subplanes can be identified and categorized within a projective plane of order nine, highlighting their relationship with specific components of a left nearfield of order nine.

Fano configurations within 5-dimensional projective spaces over GF(2) are identified and analyzed in [5]. The simplest Cartesian Group approaches to classifying *(k,3)*-arcs in projective planes of order nine and twenty-five are detailed in [6, 7]. In PG(2,5), Altıntaş and Bayar examines *(k,2)*-arcs defined over GF(5), making use of a custom arc-finding algorithm developed in C# [8]. The study in [9] focuses on determining complete *(k,3)*-arcs that are linked to the Ceva configuration.

Ceva's and Menelaus' theorems are classical geometric results that establish criteria for the concurrency of lines and the collinearity of points, respectively. In projective geometry, Menelaus's Theorem is a fundamental result that provides a criterion for collinearity of three points that lie on the sides (or their extensions) of a triangle. The theorem generalizes its classical Euclidean counterpart to the projective context, maintaining its validity under projective transformations. By incorporating directed ratios, it captures orientation and thus plays a fundamental role in projective geometry, where incidence structures and cross-ratios are preserved under transformations.

Beyond its classical form, Menelaus' Theorem holds a significant position in the study of harmonic sets and perspective transformations, thereby reinforcing its duality with Ceva's Theorem within projective configurations. Its foundational contribution to the understanding of collinearity and incidence relations makes it an indispensable element of modern projective geometry, with far-reaching influence on both theoretical advancements and applied fields.

In the recent generalization proposed by Benyi and Curgus [11], the classical theorems of Ceva and Menelaus are extended to simultaneously characterize both the collinearity of points and the concurrency of lines determined by six points located on the sides of a triangle. These generalized results highlight the deep geometric structure underlying the classical theorems, which continue to find rich applications in both projective and Euclidean geometries.

The theorems of Ceva and Menelaus are classical and well-established results. However, they describe inherently projective properties—concurrency in Ceva's Theorem and collinearity in Menelaus's Theorem—using affine concepts. In an effort to bridge this conceptual gap, Benitez proposes an alternative approach. Specifically, the study utilizes the cross ratio, a fundamentally projective invariant, to characterize the concurrence of cevians, thereby providing a more intrinsically projective formulation [12]. Menelaus' Theorem can be reformulated in a purely projective context by applying the dual of its classical characterization. Nicolae investigates the Ceva–Menelaus transformation, which maps a line into four distinct curves—specifically, a parabola, a hyperbola, or a bean-shaped ellipse. Remarkably, each of the triangle's three sides is tangent to all resulting conics. Additionally, the study reveals that the harmonic transform of a cevian does not yield an envelope; instead, it forms a pencil of lines radiating from a single point [13].

Menelaus and Ceva theorems in projective planes $P_2(F)$, where F is the field of characteristic not equal to two, were given by Kelly B. Funk [14]. Menelaus and Ceva 6-figures were first introduced within the framework of Moufang projective planes by Kaya and Çiftçi [15]. Subsequently, these configurations were explored in the context of fibered geometry in [16], where the points and lines of the underlying geometry were assigned multiple degrees of membership. Building upon classical projective geometry, the study by Akça et al. [17] extends these results by formulating intuitionistic fuzzy projective versions of the Menelaus and Ceva conditions.

This study aims to construct and classify complete *(11,3)-arcs* in the projective plane *PG(2,5)* that incorporate a Menelaus configuration. Utilizing a computational algorithm implemented in C#, the research identifies candidate points external to the Menelaus structure and systematically categorizes them according to their incidences with 0-secant, 1-secant, and 2-secant lines. Based on this classification, two distinct construction strategies are proposed, resulting in the discovery of eighteen distinct complete *(11,3)-arcs*. The findings underscore the utility of secant line distributions in guiding the structured construction of arcs within the context of finite projective geometry.

PRELIMINARIES

This section introduces fundamental concepts in projective geometry, such as projective planes, finite fields, the Menelaus configuration, and the essential properties of arcs. It covers the definition of projective planes over finite fields, the representation of points and lines, and key characteristics of arcs. These foundational elements establish the theoretical basis for the present study.

Definition 1. In a projective plane *(N, D, ∘)*, the set *N* represents points and *D* denotes lines (subsets of *N*), with the following axioms holding: every pair of points lies on one and only one line, each pair of distinct lines meets at exactly one point, and there are four non-collinear points, no three of which lie on a common line.

Definition 2. The vector space *V(n+1,q)* is *(n+1)*-dimensional and consists of vectors with coordinates from the finite field *GF(q)*. The projective space *PG(n,q)* is defined as the collection of points, each corresponding to a line that passes through the origin in *V(n+1,q)*. Specifically, this means that each point in *PG(n,q)* can be represented as *P(x)*, where x is any non-zero vector in *V(n+1,q)*. If K is the finite field *GF(q),* also denoted as F_q, then the n-dimensional projective plane is referred to as *PG(n,K)* or *PG(n,q)*. In this context, q represents the order of *PG(n,q)*. The number of points in this projective plane can be determined using the formula

$$\theta(n) = \frac{q^{n+1}-1}{q-1}.$$

$(x_1, x_2, \ldots, x_n)$ represents a point in N, where $x_1, x_2, \ldots, x_n$ are not all zero, and $(\lambda x_1, \lambda x_2, \ldots, \lambda x_n) \equiv (x_1, x_2, \ldots, x_n)$, $\lambda \in K\backslash\{0\}$. Similarly, the notation $[a_1, a_2, \ldots, a_n]$ denotes any line in D, where $a_1, a_2, \ldots, a_n$ are not all zero. The relationship $[\mu a_1, \ldots, \mu a_n] \equiv [a_1, \ldots, a_n]$ holds for $\mu \in K\backslash\{0\}$. The projective plane P_2K is characterized as a point-line geometry $(N, D, \circ)$ defined by K. The incidence relation is given by $\circ$:

$(x_1, \ldots, x_n) \circ [a_1, \ldots, a_n] \Longleftrightarrow a_1x_1 + a_2x_2 + a_3x_3 + \ldots + a_nx_n = 0$

Let p denote a prime number and r a positive integer. The projective plane of order q = p^r over the finite field $K = GF(p^r)$, where p^r represents the number of elements, is expressed as $P_2K = PG(2, p^r)$ [18].

Theorem 1. Let $\mathcal{P}$ be a projective plane. A 6-figure in $\mathcal{P}$ is a sequence of six distinct points $(A_1A_2A_3, B_1B_2B_3)$ such that $A_1A_2A_3$ constitutes a nondegenerate triangle with $B_1 \in \langle A_2, A_3 \rangle, B_2 \in \langle A_1, A_3 \rangle$, and $B_3 \in \langle A_1, A_2 \rangle$. The points $A_1, A_2, A_3, B_1, B_2, B_3$ are called vertices of this 6-figure. Such a configuration is said to be a Menelaus 6-figure if B_1, B_2, and B_3 are collinear [16].

Definition 4. In a projective plane, a set K of k points is called a *(k,n)*-arc if no line intersects K in more than n points, and at least one line meets it in precisely *n* points, with *n ≥ 2* [19].

Definition 5. A line *l* in a projective plane is defined as an *μ-secant* of a *(k,n)*-arc K if it intersects K at μ points. Let τ_i represent the total number of *i-secants* to K. The notations σ_i or $\sigma_i(Q)$ denote the count of i-secants to the set K that pass through a point Q, which is part of $P \backslash K$. A point Q is classified as an index zero point if the condition $\sigma_n(Q) = 0$ holds [20].

If there is no *(k+1,n)*-arc that contains a *(k,n)*-arc, then the *(k,n)*-arc is considered complete [20].

Definition 6. Let K be a (k, n) −arc in a projective plane. A point not contained in K but lying on an *i*-secant of K —that is, a line intersecting K in exactly *i* distinct points—is called a point of index *i* [20].

THE PROJECTIVE PLANE OF ORDER 5

The study considers *PG(2,5)*, which is built over *GF(5)* using the irreducible polynomial $f(x) = x^3 + 2x^2 + x - 1$. The elements of GF(5) with thirty one points and thirty one lines are 0, 1, 2, 3, and 4. In the projective plane order five, every line consists of six points, and each point is associated with six lines that pass through it [21].

The projective plane of order five has a point set N defined as $N = \{N_i | i = 1, 2, \ldots, 31\}$ where

$N_1 = (0,0,1)$, $N_2 = (1,1,1)$, $N_3 = (1,2,2)$, $N_4 = (1,4,2)$, $N_5 = (1,4,3)$,
$N_6 = (1,3,4)$, $N_7 = (1,0,3)$, $N_8 = (1,3,1)$, $N_9 = (1,2,4)$, $N_{10} = (1,0,4)$,
$N_{11} = (1,0,1)$, $N_{12} = (1,2,1)$, $N_{13} = (1,2,3)$, $N_{14} = (1,3,0)$, $N_{15} = (0,1,3)$,
$N_{16} = (1,1,3)$, $N_{17} = (1,3,3)$, $N_{18} = (1,3,2)$, $N_{19} = (1,4,0)$, $N_{20} = (0,1,4)$,
$N_{21} = (1,1,0)$, $N_{22} = (0,1,1)$, $N_{23} = (1,1,2)$, $N_{24} = (1,4,4)$, $N_{25} = (1,0,2)$,
$N_{26} = (1,4,1)$, $N_{27} = (1,2,0)$, $N_{28} = (0,1,2)$, $N_{29} = (1,1,4)$, $N_{30} = (1,0,0)$,
and $N_{31} = (0,1,0)$.

Table 1 presents the incidence relation between the points and the lines in the projective plane *PG(2,5)*. In this table, each row corresponds to a specific line, denoted as D_i, where i ranges from 1 to 31. For each line D_i, the table lists the points on that line.

Table 1. The points and lines based on incidence relation

D_1	N_2	N_3	N_{17}	N_{22}	N_{24}	N_{30}
D_2	N_3	N_4	N_{18}	N_{23}	N_{25}	N_{31}
D_3	N_4	N_5	N_{19}	N_{24}	N_{26}	N_1
D_4	N_5	N_6	N_{20}	N_{25}	N_{27}	N_2
D_5	N_6	N_7	N_{21}	N_{26}	N_{28}	N_3
D_6	N_7	N_8	N_{22}	N_{27}	N_{29}	N_4
D_7	N_8	N_9	N_{23}	N_{28}	N_{30}	N_5
D_8	N_9	N_{10}	N_{24}	N_{29}	N_{31}	N_6
D_9	N_{10}	N_{11}	N_{25}	N_{30}	N_1	N_7
D_{10}	N_{11}	N_{12}	N_{26}	N_{31}	N_2	N_8
D_{11}	N_{12}	N_{13}	N_{27}	N_1	N_3	N_9
D_{12}	N_{13}	N_{14}	N_{28}	N_2	N_4	N_{10}
D_{13}	N_{14}	N_{15}	N_{29}	N_3	N_5	N_{11}
D_{14}	N_{15}	N_{16}	N_{30}	N_4	N_6	N_{12}
D_{15}	N_{16}	N_{17}	N_{31}	N_5	N_7	N_{13}
D_{16}	N_{17}	N_{18}	N_1	N_6	N_8	N_{14}
D_{17}	N_{18}	N_{19}	N_2	N_7	N_9	N_{15}
D_{18}	N_{19}	N_{20}	N_3	N_8	N_{10}	N_{16}
D_{19}	N_{20}	N_{21}	N_4	N_9	N_{11}	N_{17}
D_{20}	N_{21}	N_{22}	N_5	N_{10}	N_{12}	N_{18}
D_{21}	N_{22}	N_{23}	N_6	N_{11}	N_{13}	N_{19}
D_{22}	N_{23}	N_{24}	N_7	N_{12}	N_{14}	N_{20}
D_{23}	N_{24}	N_{25}	N_8	N_{13}	N_{15}	N_{21}
D_{24}	N_{25}	N_{26}	N_9	N_{14}	N_{16}	N_{22}
D_{25}	N_{26}	N_{27}	N_{10}	N_{15}	N_{17}	N_{23}

D_{26}	N_{27}	N_{28}	N_{11}	N_{16}	N_{18}	N_{24}
D_{27}	N_{28}	N_{29}	N_{12}	N_{17}	N_{19}	N_{25}
D_{28}	N_{29}	N_{30}	N_{13}	N_{18}	N_{20}	N_{26}
D_{29}	N_{30}	N_{31}	N_{14}	N_{19}	N_{21}	N_{27}
D_{30}	N_{31}	N_1	N_{15}	N_{20}	N_{22}	N_{28}
D_{31}	N_1	N_2	N_{16}	N_{21}	N_{23}	N_{29}

INVESTIGATION OF COMPLETE (10,3)-ARCS BASED ON THE MENELAUS CONFIGURATION IN PG(2,5)

This section presents an algorithm used to construct complete (11,3)-arcs by including the Menelaus configuration and utilizing secant distributions in PG(2,5).

Two different methods are applied to obtain a total of eighteen different complete (11,3)-arcs:

        Method 1. → contructs twelve different complete (11,3)-arcs

        Method 2. → contructs six different complete (11,3)-arcs

Each method follows a structured approach, ensuring systematic identification and completion of arcs.

Methodology: Constructing (11,3)-Arcs in PG(2,5)

This section presents an algorithm designed to construct (11,3)-arcs, incorporating the Menelaus configuration and utilizing secant distributions in PG(2,5). The algorithm follows a structured approach, ensuring systematic identification and extension of arcs.

Step 1: Initialization and Projective Plane Definition

- Identify the points and lines of *PG(2,5)* using the irreducible polynomial
$$f(x) = x^3 + 2x^2 + x - 1 \text{ over } GF(5).$$
- Applying this polynomial, determine *31* points and *31* lines in the projective plane (see Table 1).
- Store the identified points and lines in dataset A.

Step 2: Definition of the Menelaus Configuration

- Consider a Menelaus configuration M in PG(2,5), consisting of six points: $M = \{A_1, A_2, A_3, B_1, B_2, B_3\}$.
- *M* forms an incomplete *(6,3)*-arc in *PG(2,5)*.

Step 3: Determination of Remaining Points

- Identify 13 points that do not lie on the lines of M.
- Classify these 13 points into three categories based on their secant line properties to Menalaus configuration M in PG(2,5):

1. Category 1: Six points have
   - One 0-secant line
   - Four 1-secant lines
   - One 2-secant line
2. Category 2: Four points have
   - Six 1-secant lines
3. Category 3: Three points have
   - Two 0-secant lines
   - Two 1-secant lines
   - Two 2-secant lines

Step 4: Construction of the Triangle

- Category 3 points define a triangle in PG(2,5):
$$C_1 = A_1B_1 \cap A_2B_2,$$
$$C_2 = A_1B_1 \cap A_3B_3,$$
$$C_3 = A_2B_2 \cap A_3B_3.$$
where $\sigma_2(C_j) = 2, \sigma_1(C_j) = 2, \sigma_0(C_j) = 2, j = 1, 2, 3$.

- Each edge of this triangle intersects the Menelaus configuration at two points.
- The triangle $C_1C_2C_3$ such that the points C_1, C_2, C_3 of this triangle are with 2 -index out of M.

Step 5: First Method – Constructing complete (11,3)-Arcs using $\sigma_2(D_k) =1, k=1,2,…6$

The points D_k lie in pairs on the sides of the triangle $C_1C_2C_3$.

Step 5.1. Constructing the (8,3)-Arc
- Select one point from the points D_k which are on each of two sides of a triangle $C_1C_2C_3$ belonging to Category 1 and add it to M, then an incomplete (8,3)-arc is obtained as $M_1 = M \cup \{D_i, D_j\}$, where $i,j \in \{1,2,…,6\}$ and $i \neq j$.
- While Category 2 initially contains four points with $\sigma_1(E_t)=6$, $t=1,2,3,4$, the application of the algorithm leaves only three of them, which can subsequently be added to the arc M_1.

Step 5.2. Constructing the (11,3)-Arc

- A complete (11,3)-arc is obtained by adding the three remaining points E_t in Category 2 to the incomplete (8,3)-arc M_1 determined in Step 5.1 as $M_2 = M_1 \cup \{E_i, E_j, E_k\}$, where $i, j, k \in \{1,2,3,4\}$ and $i \neq j \neq k$.

Step 6: Second Method - Constructing complete (11,3)-Arcs using $\sigma_1(E_t)=6$, $t=1,2,\dots4$

Step 6.1: Constructing the (10,3)-Arc

- After Step 2 is applied, four distinct points E_t in Category 2 remain. none of which lie on the sides of the triangle $C_1 C_2 C_3$. If the points $E_t, t = 1,2,3,4$ are added to the (6,3)-arc M, an incomplete (10,3)-arc is obtained as $M_1 = M \cup \{E_1, E_2, E_3, E_4\}$.

Step 6.2: Constructing the (11,3)-Arc

- If the algorithm is applied to the incomplete (10,3)-arc M_1, there are six remaining points D_k defined as $\sigma_2(D_k) = 1$, $k=1,2,\dots6$ that can be added to the incomplete (10,3)-arc. By selecting one point of these six points $D_k, k = 1,2,\dots6$ and adding it to M_1, a complete (11,3)-arc is obtained.

Algorithm Implementation

We present the following algorithm, implemented in C#, designed to identify complete *(k,3)-arcs* within *PG(2,5):*

```
A ← Read(Excel File)
B ← Read(Text File)
C ← A
while s(C)>0
  B_i ← input(b), {b|b ∈ C, b ∉ B, i = s(B) + 1}
  j=1
  while j ≤ s(B)
    for k=(j+1) to s(B)
      m ← the index of row on B_j, B_k
      D ← A_mn; {A_mn|A_mn ≠ B_j, A_mn ≠ B_k, n = 1,…,10 }
      Remove a from A; {a|a ∈ A, a ∈ D}
      C ← c; {c|c ∈ A, c ∉ C}
    end for
    j=j+1
  end while
end while
```

Theorem 2. Menelaus configuration determines an incomplete (6,3)-arc in *PG(2,5)*.

Proof. Let $M = \{A_1, A_2, A_3, B_1, B_2, B_3\}$ be any Menelaus configuration in *PG(2,5)*. M contains six lines and six points. From Theorem 1, since no four points in the Menelaus configuration are collinear, the set of these points forms a (6,3)-arc. From Definition 5, this (6,3)-arc is not complete.

Now, if the given algorithm is applied to the points of the incomplete (6,3)-arc determined by Menelaus configuration to find (k,3)-arcs, then there are thirteen remaining points.

Theorem 3. There are eighteen different complete *(11,3) −arcs* containing a Menelaus configuration in *PG(2,5)*.

Proof. Let *M* be a Menelaus configuration. From Theorem 2, *M* is an incomplete *(6,3)-arc* in *PG(2,5)*. If the given algorithm is applied to *M* to find (k,3)-arcs, there are thirteen remaining points which are classified into three categories based on their secant lines. Nine of these thirteen remaining points are 2-index points. Among them, three points C_j have $\sigma_2(C_j) = 2, j = 1, 2, 3$, six points D_k have $\sigma_2(D_k) = 1, k = 1, 2, ..., 6$, and four points E_t have $\sigma_1(E_t) = 6$, $l = 1, 2, ...4$. When the Menelaus configuration and these categories are examined, it is observed that the points C_1, C_2, C_3 in Category 3 have two 2-secant lines and form a triangle $C_1 C_2 C_3$ as $A_1 B_1 \cap A_2 B_2 = C_1, A_1 B_1 \cap A_3 B_3 = C_2, A_2 B_2 \cap A_3 B_3 = C_3$.

And also, there are six non-vertex points located on two sides of a triangle that do not belong to the Menelaus configuration. These remaining points $D_k, k = 1, 2, ..., 6$ are positioned in pairs on the edges of the triangle as follows: $D_1, D_5 \circ C_1 C_3, D_2, D_6 \circ C_2 C_3, D_3, D_4 \circ C_1 C_2$.

Now, the proof continues by applying the construction method introduced in Step 5, beginning with the selection of two suitable points D_k from different sides of the triangle $C_1 C_2 C_3$ to extend the Menelaus configuration.

i) If one point from each of two different sides of the triangle $C_1 C_2 C_3$ is selected (e.g., D_1, D_2) and added to *M*, and the algorithm is applied, then an incomplete (8,3)-arc M_1 is obtained, where $M_1 = M \cup \{D_1, D_2\} = \{A_1, A_2, A_3, B_1, B_2, B_3, D_1, D_2\}$. After D_1 and D_2 are added, three more points remain from the set $E_t, t = 1, 2, 3, 4$ in Category 2, that can be added to M_1. Every line passing through any of these points intersects the Menelaus configuration at exactly one point. Consequently, when any three of the points E_t are added to M_1, an (11,3)-arc $M_2 = M_1 \cup \{E_1, E_2, E_3\}$ is obtained. There is no remaining point that can be added to M_2, so M_2 is a complete (11,3)-arc.

Since two points from among the D_k set can be selected in twelve different ways, applying this method to all such combinations results in twelve distinct complete (11,3)-arcs.

In the second part of the proof, we apply the construction method described in Step 6, which focuses on extending the arc by first adding points from Category 2 that do not lie on the triangle's sides.

ii) Consider the points E_t, that can be added and do not lie on the sides of the triangle. These four points belong to Category 2. The triangle $C_1 C_2 C_3$ is the diagonal triangle of the complete quadrangle $E_1 E_2 E_3 E_4$. First, let us add all four of these points E_t to M, then $M \cup \{E_1, E_2, E_3, E_4\}$ forms an incomplete (10,3)-arc, denoted by M_1. When the algorithm is applied to M_1, six points remain which are D_k, $k = 1,2,\dots,6$. When any one from the set D_k is added to M_1, an (11,3)-arc $M_2 = M_1 \cup \{D_k\}, k = 1,2,\dots,6$ is obtained. Since only one secant passes through the added point, no additional point can be added to the arc. Thus the resulting (11,3)-arc is complete.
Applying all possible selections of D_k within Category 1 yields six distinct complete (11,3)-arcs.
Therefore, from cases i) and ii), a total of eighteen distinct complete *(11,3)-* arcs containing a Menelaus configuration in *PG(2,5)* are obtained.

Example 1.
Let us consider the Menalaus configuration determined by the point set $M = \{N_2, N_3, N_5, N_6, N_{21}, N_{22}\}$. By applying the given algorithm to M, it is observed that M forms a *(6,3)-arc,* but it is incomplete. In this projective plane, the points lying on the lines spanned by *(6,3)-arc* are removed from the point set of *PG(2,5),* and the remaining points are $N_1, N_4, N_8, N_9, N_{11}, N_{13}, N_{14}, N_{15}, N_{16}, N_{19}, N_{23}, N_{29}, N_{31}$. Since six lines pass through each of these points in PG(2,5), they can be classified into three categories based on their secant line properties. Table 2 presents the 0-secant, 1-secant, and 2-secant lines of the Menelaus configuration that pass through the points outside of M in PG(2,5).

Table 2. The remaining points and the secant lines of the Menalaus configuration

Category Type	Point	0-secant	1-secant	2-secant
Category 1	N_1	D_9	$D_3, D_{11}, D_{16}, D_{30}$	D_{31}
	N_{13}	D_{28}	$D_{11}, D_{12}, D_{15}, D_{23}$	D_{21}
	N_{14}	D_{22}	$D_{12}, D_{16}, D_{24}, D_{29}$	D_{13}
	N_{15}	D_{25}	$D_{14}, D_{17}, D_{23}, D_{30}$	D_{13}
	N_{16}	D_{26}	$D_{14}, D_{15}, D_{18}, D_{24}$	D_{31}
	N_{19}	D_{27}	$D_3, D_{17}, D_{18}, D_{29}$	D_{21}

Category 2	N_4		$D_2, D_3, D_6, D_{12}, D_{14}, D_{19}$	
	N_8		$D_6, D_7, D_{10}, D_{16}, D_{18}, D_{23}$	
	N_9		$D_7, D_8, D_{11}, D_{17}, D_{19}, D_{24}$	
	N_{31}		$D_2, D_8, D_{10}, D_{15}, D_{29}, D_{30}$	
Category 3	N_{11}	D_9, D_{26}	D_{10}, D_{19}	D_{13}, D_{21}
	N_{23}	D_{22}, D_{25}	D_2, D_7	D_{21}, D_{31}
	N_{29}	D_{27}, D_{28}	D_6, D_8	D_{13}, D_{31}

When these categories are examined, it is observed that the points in Category 3 have two 2-secant lines and form a triangle $N_{11}N_{23}N_{29}$. The edges of this triangle intersect the Menelaus configuration at two points.

According to Method 1, if one point from each of two different sides of the triangle $N_{11}N_{23}N_{29}$ is selected (e.g., N_1, N_{13}) and added to $M = \{N_2, N_3, N_5, N_6, N_{21}, N_{22}\}$, and then the algorithm is applied, an incomplete (8,3)-arc is obtained as $M_1 = \{N_1, N_2, N_3, N_5, N_6, N_{13}, N_{21}, N_{22}\}$. At this stage, three points N_4, N_8, N_{31} remain from Category 2 that can be added to M_1. Every line passing through any of these points intersects the Menelaus configuration at exactly one point. Consequently, when the points N_4, N_8, N_{31} are added to M_1, then an (11,3)-arc is obtained as $M_2 = M_1 \cup \{N_4, N_8, N_{31}\}$. There is no remaining point that can be added to M_2, so M_2 is a complete (11,3)-arc.

According to Method 2, if the points N_4, N_8, N_9, N_{31}, which do not lie on the sides of the triangle, and belong to Category 2, are selected and added to M, and the algorithm is applied, an incomplete (10,3)-arc is obtained as $M_1 = M \cup \{N_4, N_8, N_9, N_{31}\} = \{N_2, N_3, N_4, N_5, N_6, N_8, N_9, N_{21}, N_{22}, N_{31}\}$. Then six points $N_1, N_{13}, N_{14}, N_{15}, N_{16}, N_{19}$ remain, all belonging to Category 1. If one of these remaining Category 1 points (e.g., N_1) is added to the incomplete (10,3)-arc M_1, the complete (11,3)-arc is obtained as $M_2 = M_1 \cup \{N_1\} = \{N_1, N_2, N_3, N_4, N_5, N_6, N_8, N_9, N_{21}, N_{22}, N_{31}\}$.

Based on the example above, all complete (11,3)-arcs that can be constructed from all possible configurations of the remaining points—using both Method 1 and Method 2—are listed in Table 3, resulting in a total of eighteen distinct complete (11,3)-arcs containing the Menelaus configuration $M = \{N_2, N_3, N_5, N_6, N_{21}, N_{22}\}$ in *PG(2,5)*.

Table 3. Complete (11,3)-arcs

Completion of (6,3)-arc	Complete (10,3)-arcs
M $\cup \{N_1, N_4, N_8, N_9, N_{15}\}$	$\{N_1, N_2, N_3, N_4, N_5, N_6, N_8, N_9, N_{15}, N_{21}, N_{22}\}$
M $\cup \{N_1, N_4, N_8, N_9, N_{31}\}$	$\{N_1, N_2, N_3, N_4, N_5, N_6, N_8, N_9, N_{21}, N_{22}, N_{31}\}$
M $\cup \{N_1, N_4, N_8, N_{13}, N_{31}\}$	$\{N_1, N_2, N_3, N_4, N_5, N_6, N_8, N_{13}, N_{21}, N_{22}, N_{31}\}$
M $\cup \{N_1, N_4, N_9, N_{14}, N_{31}\}$	$\{N_1, N_2, N_3, N_4, N_5, N_6, N_9, N_{14}, N_{21}, N_{22}, N_{31}\}$
M $\cup \{N_1, N_8, N_9, N_{19}, N_{31}\}$	$\{N_1, N_2, N_3, N_5, N_6, N_8, N_9, N_{19}, N_{21}, N_{22}, N_{31}\}$
M $\cup \{N_4, N_8, N_9, N_{13}, N_{16}\}$	$\{N_2, N_3, N_4, N_5, N_6, N_8, N_9, N_{13}, N_{16}, N_{21}, N_{22}\}$
M $\cup \{N_4, N_8, N_9, N_{13}, N_{31}\}$	$\{N_2, N_3, N_4, N_5, N_6, N_8, N_9, N_{13}, N_{21}, N_{22}, N_{31}\}$
M $\cup \{N_4, N_8, N_9, N_{14}, N_{31}\}$	$\{N_2, N_3, N_4, N_5, N_6, N_8, N_9, N_{14}, N_{21}, N_{22}, N_{31}\}$
M $\cup \{N_4, N_8, N_9, N_{14}, N_{19}\}$	$\{N_2, N_3, N_4, N_5, N_6, N_8, N_9, N_{14}, N_{19}, N_{21}, N_{22}\}$
M $\cup \{N_4, N_8, N_9, N_{15}, N_{31}\}$	$\{N_2, N_3, N_4, N_5, N_6, N_8, N_9, N_{15}, N_{21}, N_{22}, N_{31}\}$
M $\cup \{N_4, N_8, N_9, N_{16}, N_{31}\}$	$\{N_2, N_3, N_4, N_5, N_6, N_8, N_9, N_{16}, N_{21}, N_{22}, N_{31}\}$
M $\cup \{N_4, N_8, N_9, N_{19}, N_{31}\}$	$\{N_2, N_3, N_4, N_5, N_6, N_8, N_9, N_{19}, N_{21}, N_{22}, N_{31}\}$
M $\cup \{N_4, N_8, N_{14}, N_{16}, N_{31}\}$	$\{N_2, N_3, N_4, N_5, N_6, N_8, N_{14}, N_{16}, N_{21}, N_{22}, N_{31}\}$
M $\cup \{N_4, N_8, N_{15}, N_{19}, N_{31}\}$	$\{N_2, N_3, N_4, N_5, N_6, N_8, N_{15}, N_{19}, N_{21}, N_{22}, N_{31}\}$
M $\cup \{N_4, N_9, N_{13}, N_{15}, N_{31}\}$	$\{N_2, N_3, N_4, N_5, N_6, N_9, N_{13}, N_{15}, N_{21}, N_{22}, N_{31}\}$
M $\cup \{N_4, N_9, N_{16}, N_{19}, N_{31}\}$	$\{N_2, N_3, N_4, N_5, N_6, N_9, N_{16}, N_{19}, N_{21}, N_{22}, N_{31}\}$
M $\cup \{N_8, N_9, N_{13}, N_{14}, N_{31}\}$	$\{N_2, N_3, N_5, N_6, N_8, N_9, N_{13}, N_{14}, N_{21}, N_{22}, N_{31}\}$
M $\cup \{N_8, N_9, N_{15}, N_{16}, N_{31}\}$	$\{N_2, N_3, N_5, N_6, N_8, N_9, N_{15}, N_{16}, N_{21}, N_{22}, N_{31}\}$

CONCLUSION

In this study, we have systematically constructed and analyzed complete *(11,3)*-arcs in the projective plane *PG(2,5)*, each containing a Menelaus configuration. By implementing a structured algorithm in *C#*, we identified and classified the remaining points outside the Menelaus configuration based on their secant properties, particularly focusing on the distribution of *0-secant, 1-secant,* and *2-secant* lines. Through this classification, we introduced two distinct methods that together yielded a total of eighteen different complete *(11,3)*-arcs.

The first method focused on the triangle formed by Category 3 points with two *2*-secant lines. Here in, we utilized the structured placement of index-*2* points on the sides of this triangle. By selecting one point from each of two different sides of the triangle and then adding the three remaining point in Category 2, twelve complete *(11,3)*-arcs were obtained.

The second method focused on the points out of the sides of the triangle, resulting in six distinct complete *(11,3)*-arcs. By adding all remaining points not on the triangle with index-1 and then adding one point from six remaining point in Category 1, six complete *(11,3)*-arcs were obtained. As a result, a total of eighteen different complete *(11,3)*-arcs containing a Menelaus configuration are identified in *PG(2,5)*.

This work contributes to the structural understanding of arcs derived from classical configurations in finite projective geometry and offers a computational approach to their classification.

REFERENCES

[1] J.W.P. Hirschfeld and J.A. Thas, "General Galois Geometries," *Springer Monographs in Mathematics*. Springer- Verlag London, 2016.

[2] A. Bayar, Z. Akca, E. Altintas, and S. Ekmekci, S. "On the complete arcs containing the quadrangles constructing the Fano planes of the left near field plane of order 9," *New Trend Math. Sci.*, 4(4), 266-266, 2016. http://dx.doi.org/10.20852/ntmsci.2016.113

[3] S. Ekmekci, A. Bayar, E. Altintas, and Z. Akca, "On the Complete (k,2)- Arcs of the Hall Plane of Order 9," *IJARCSSE*, 6 (10), 282-288, 2016. ISSN: 2277 128X.

[4] Z. Akca, S. Ekmekci, and A. Bayar, "On Fano Configurations of the Left Hall Plane of order 9," *Konuralp J. Math.,* 4 (2), 116-123, 2016.

[5] Z. Akca, and A. Altıntas, "A Note on Fano Configurations in the Projective Space PG(5,2)," *Konuralp J. Math.,* 9(1), 190-192, 2021.

[6] Z. Akca, "A numerical computation of (k, 3)-arcs in the left semifield plane order 9*", Int. Electron. J. Geom.*, 4(2), 13-21, 2011.

[7] Z. Akca, and I. Günaltılı, I. "On the (k, 3)- arcs of CPG (2,25,5)," *Anadolu Univ J Sci Technol J Theor Sci,* 1(0), 21-27, 2012.

[8] E. Altıntas, and A. Bayar, "Complete (k,2)-Arcs in the Projective Plane Order 5," *HSJG*, 5(1), 11-14, 2023. e-ISSN 2687-4261.

[9] E. Altıntaş Kahriman, A. Bayar, "On (k,3)-arcs derived by Ceva configurations in PG(2,5)," *Journal of Scientific Reports-A*, 059, 10–18, 2024, doi: 10.59313/jsr-a.1559383.

[11] V. Danos, and L. Regnier, "The structure of multiplicatives," *Arch Math Logic*, 28, 181-203, 1989. https://doi.org/10.1007/BF01622878
[12] J. Benitez, "A unified proof of Ceva and Menelaus' theorems using projective geometry," *JGG*, 11(1):39–44, 2007. ISSN 1433-8157
[13] V. Nicolae, "On The Ceva's And Menelaus's Theorems." *Rom. J. Phys.,* [S.l.], v. 5, n. 2, p. 43-50, 2020. ISSN 2537-5229.
[14] B.K. Funk, "Ceva and Menelaus in projective geometry," University of Louisuille, 42 p, 2008.
[15] S. Çiftçi, R. Kaya, and J.C. Ferrar, "On Menelaus and Ceva 6-figures in Moufang projective planes," *Geom. Dedicata*, vol. 19, no. 3, pp. 295–296, 1985.
[16] A. Bayar, and S. Ekmekçi, "On the Menelaus and Ceva 6-figures in the fibered projective planes," *Abstr. Appl. Anal.*,1-5, 2014. 10.1155/2014/803173
[17] Z. Akça, A. Bayar, and S. Ekmekçi, "On the intuitionistic fuzzy projective Menelaus and Ceva's conditions," *Commun. Fac. Sci. Univ. Ank. Ser. A1 Math. Stat.,* 69(1), 891-899, 2020. https://doi.org/10.31801/cfsuasmas.567753.
[18] J.W.P. Hirschfeld, and J.A. Thas, "General Galois Geometries," *The Charendon Press*, Oxford, 1991.

[19] J.W.P. Hirschfeld, and J.F. Voloch, "Group-arcs of prime order on cubic curves," *Finite Geometry and Combinatorics*, 191, 177-185, 2015.

[20] J.W.P. Hirschfeld, and E.V.D. Pichanick "Bounded for arcs of arbitrary degree in finite Desarguesian Planes" *J Comb Des.,* 24(4), 184-196, 2016.

[21] B.A. Qassim, "The construction for the arcs (8,4)-from the two arcs (7,4)-in PG (2,q), q=5," *J. Phys. Conf. Ser.,* 1664012039, 2020.

Complete (10,3)-Arcs Constructed from Menelaus Configurations in PG(2,5): A Secant-Based Approach

Elif ALTINTAŞ KAHRİMAN [1]
Ayşe BAYAR[2]

1- Assist Prof. ; Bartın University, Department of Management Information System, Bartın University, Faculty of Economics and Administrative Sciences,. ealtintaskahriman@bartin.edu.tr ORCID No: 0000-0002-3454-0326

2- Prof. ; Eskişehir Osmangazi University, Department of Mathematics and Computer Sciences, Eskişehir Osmangazi University, Faculty of Science,. akorkmaz@ogu.edu.tr ORCID No: 0000-0002-2210-5423

ABSTRACT

This study investigates complete *(10,3)*-arcs in the projective plane *PG(2,5)* that contain a Menelaus configuration. By developing and implementing a computational algorithm in C#, we construct and classify complete arcs through a detailed analysis of the secant line distributions associated with the Menelaus configuration. The algorithm identifies thirteen points outside the Menelaus set, which are grouped into three distinct categories based on their incidence with 0-secant, 1-secant, and 2-secant lines. Two different methods are proposed to construct complete *(10,3)*-arcs: the first method produces twenty-four arcs by extending the triangle formed by points with two 2-secant lines; the second method yields eight additional arcs through a structured selection of points on the triangle edges. As a result, a total of thirty-two distinct complete *(10,3)*-arcs are obtained. This work highlights the geometric and combinatorial structure of the Menelaus configuration in finite projective planes and offers a practical algorithmic approach for the classification and construction of complete arcs in *PG(2,5)*.

Keywords – projective plane; (k,3)-arc; Menelaus configuration; secant lines; finite geometry; PG(2,5)

INTRODUCTION

Arcs play a crucial role in projective geometry and find numerous applications in combinatorics and allied fields. A *k*-arc is defined as a set *K* of *k* points (where $k \geq 3$) that are not all located on the same line in a finite projective plane *π*. A hyperoval is defined as a *(p+2)*-arc. The highest value of k can be achieved only when *p* is even, while k $\geq$ p+2 if the plane π has an order of p. In the literature, ovals are a common topic, and Hirschfeld is often cited in this context [1]. Research on arcs in projective planes is extensive, particularly regarding complete *(k,2)*-arcs that create complete quadrangles, leading to Fano planes in the projective plane, as analyzed in [2, 3]. The identification and classification of Fano subplanes in a projective plane of order nine, related to parts of a left nearfield of order nine, are described in [4].

Fano configurations in *5*-dimensional projective spaces over *GF(2)* are discovered in [5]. In the projective planes of order nine and twenty-five, the simplest Cartesian Group techniques for classifying (k,3)-arcs are outlined in references [6, 7]. The research by Altıntaş investigates (k,2)-arcs in *PG(2,5),* coordinated by elements from *GF(5),* using an arc-finding algorithm developed in *C#* [8]. The determination of complete *(k,3)*−arcs related to the Ceva configuration is presented in [9].

Ceva's and Menelaus' theorems are fundamental results in geometry, characterizing the conditions for concurrency of lines and collinearity of points, respectively. In projective geometry, Menelaus's Theorem is a fundamental result that provides a criterion for collinearity of three points that lie on the sides (or their extensions) of a triangle. It extends the classical Euclidean version into a projective setting, where it remains valid under projective transformations. This directed ratio condition accounts for orientation, making the theorem fundamental in projective geometry, where incidence relations and cross-ratios are preserved under transformations.

Beyond its classical formulation, Menelaus' Theorem plays a crucial role in harmonic sets and perspective transformations, reinforcing its duality with Ceva's Theorem in projective configurations.

Its foundational role in collinearity and incidence relations makes it an essential tool in modern projective geometry, influencing both theoretical developments and practical applications.

In the recent Benyi-Curgus generalization of the theorems of Ceva and Menelaus [11], both the collinearity of points and the concurrence of straightlines specified by six points on the edges of a triangle are characterized. Both Menelaus's and Ceva's theorems have intriguing applications in projective and Euclidean geometries.

Theorems of Ceva and Menelaus are well-known conclusions. However, these theorems characterize a projective property through an affine property: concurrency in Ceva's theorem and collinearity in Menelaus' theorem. Benitez aims to get over this, therefore. In particular, the cross ratio a projective quantity is used in the study to characterize the concurrence of the cevians [12]. One can express Menelaus' theorem in a projective form by using the dual of this latter characterization. Nicolae discusses the Ceva-Menelaus transformation of a line into four curves. This proved to be a parabola, a hyperbola, or a bean ellipse. The triangle's three straight lines are tangent to each of the conics. Furthermore, in the study the harmonic transform for a ceviana has no envelope since it is a beam of straight lines flowing through a point is discovered [13].

Menelaus and Ceva theorems in projective planes $P_2(F)$, where F is the field of characteristic not equal to two, were given by Kelly B. Funk [14]. Menelaus and Ceva 6-figures were first introduced in Moufang projective planes by Kaya and Çiftçi in [15]. Menelaus and Ceva's 6-figures in fibered geometry were examined in [16] with multiple degrees of membership of the points and lines of the basic geometry. The study by Akça et al. provides intuitionistic fuzzy projective versions of Menelaus and Ceva's conditions, based on a classical projective plane. [17].

The main objective of this study is to construct and classify complete $(10,3)$−arcs in the projective plane $PG(2,5)$ which contain a Menelaus configuration. By applying a computational algorithm developed in C#, the study identifies the points outside the Menelaus configuration and categorizes

them based on their secant line incidences—specifically, their interaction with 0-secant, 1-secant, and 2-secant lines. Leveraging this classification, two different construction methods are introduced, which lead to the identification of thirty-two distinct complete *(10,3)−* arcs. This approach highlights how secant line distributions can be effectively utilized in the systematic construction of arcs in finite projective geometry.

PRELIMINARIES

This section outlines key concepts in projective geometry, including projective planes, finite fields, Menelaus configuration and arc properties. We define projective planes over finite fields, the representation of points and lines, and the properties of arcs. These definitions provide the foundation for our study.

Definition 1. In a projective plane *(N, D, ∘)*, the set *N* represents points and *D* denotes lines (subsets of *N*), with the following axioms holding: every pair of points lies on one and only one line, each pair of distinct lines meets at exactly one point, and there are four non-collinear points, no three of which lie on a common line.

Definition 2. The vector space *V(n+1,q)* is *(n+1)*-dimensional and consists of vectors with coordinates from the finite field *GF(q)*. The projective space *PG(n,q)* is defined as the collection of points, each corresponding to a line that passes through the origin in *V(n+1,q)*. Specifically, this means that each point in *PG(n,q)* can be represented as *P(x)*, where x is any non-zero vector in *V(n+1,q)*. If K is the finite field *GF(q)*, also denoted as F_q, then the n-dimensional projective plane is referred to as *PG(n,K)* or *PG(n,q)*. In this context, q represents the order of *PG(n,q)*. The number of points in this projective plane can be determined using the formula

$$\theta(n) = \frac{q^{n+1}-1}{q-1}.$$

$(x_1, x_2, \ldots, x_n)$ represents a point in N, where $x_1, x_2, \ldots, x_n$ are not all zero, and $(\lambda x_1, \lambda x_2, \ldots, \lambda x_n) \equiv (x_1, x_2, \ldots, x_n)$, $\lambda \in K\backslash\{0\}$. Similarly, the notation $[a_1, a_2, \ldots, a_n]$ denotes any line in D, where $a_1, a_2, \ldots, a_n$ are not all zero. The relationship $[\mu a_1, \ldots, \mu a_n] \equiv [a_1, \ldots, a_n]$ holds for $\mu \in K\backslash\{0\}$. The projective plane P_2K is characterized as a point-line geometry *(N, D, ∘)* defined by *K*. The incidence relation is given by ∘:

$(x_1, \ldots, x_n) \circ [a_1, \ldots, a_n] \Longleftrightarrow a_1 x_1 + a_2 x_2 + a_3 x_3 + \ldots + a_n x_n = 0$

Let *p* denote a prime number and r a positive integer. The projective plane of order q = p^r over the finite field $K = GF(p^r)$, where p^r represents the number of elements, is expressed as $P_2K = PG(2, p^r)$ [18].

Theorem 1. Let $\mathcal{P}$ be a projective plane. A 6-figure in $\mathcal{P}$ is a sequence of six distinct points $(A_1A_2A_3, B_1B_2B_3)$ such that $A_1A_2A_3$ constitutes a nondegenerate triangle with $B_1 \in \langle A_2, A_3 \rangle, B_2 \in \langle A_1, A_3 \rangle$, and $B_3 \in \langle A_1, A_2 \rangle$. The points $A_1, A_2, A_3, B_1, B_2, B_3$ are called vertices of this 6-figure. Such a configuration is said to be a Menelaus 6-figure if B_1, B_2, and B_3 are collinear [16].

Definition 4. In a projective plane, a set K of k points is called a *(k,n)-arc* if no line intersects K in more than n points, and at least one line meets it in precisely n points, with $n \geq 2$ [19].

Definition 5. A line l in a projective plane is defined as an μ-*secant* of a *(k,n)-arc* K if it intersects K at μ points. Let τ_i represent the total number of *i-secants* to K. The notations σ_i or $\sigma_i(Q)$ denote the count of i-secants to the set K that pass through a point Q, which is part of $P \setminus K$. A point Q is classified as an index zero point if the condition $\sigma_n(Q) = 0$ holds [20].

   If there is no *(k+1,n)-arc* that contains a *(k,n)-arc*, then the *(k,n)-arc* is considered complete [20].

Definition 6. Let K be a (k, n) −arc in a projective plane. A point not contained in K but lying on an *i-secant* of K —that is, a line intersecting K in exactly i distinct points—is called a point of index i [20].

THE PROJECTIVE PLANE OF ORDER 5

   The study considers *PG(2,5)*, which is built over *GF(5)* using the irreducible polynomial $f(x) = x^3 + 2x^2 + x − 1$. The elements of GF(5) with thirty one points and thirty one lines are 0, 1, 2, 3, and 4. In the projective plane order five, every line consists of six points, and each point is associated with six lines that pass through it [21].
The projective plane of order five has a point set N defined as $N = \{N_i | i = 1, 2, \ldots, 31\}$ where

$N_1 = (0,0,1), N_2 = (1,1,1), N_3 = (1,2,2), N_4 = (1,4,2), N_5 = (1,4,3),$
$N_6 = (1,3,4), N_7 = (1,0,3), N_8 = (1,3,1), N_9 = (1,2,4), N_{10} = (1,0,4),$
$N_{11} = (1,0,1), N_{12} = (1,2,1), N_{13} = (1,2,3), N_{14} = (1,3,0), N_{15} = (0,1,3),$
$N_{16} = (1,1,3), N_{17} = (1,3,3), N_{18} = (1,3,2), N_{19} = (1,4,0), N_{20} = (0,1,4),$
$N_{21} = (1,1,0), N_{22} = (0,1,1), N_{23} = (1,1,2), N_{24} = (1,4,4), N_{25} = (1,0,2),$
$N_{26} = (1,4,1), N_{27} = (1,2,0), N_{28} = (0,1,2), N_{29} = (1,1,4), N_{30} = (1,0,0),$
and $N_{31} = (0,1,0).$

Table 1 presents the incidence relation between the points and the lines in the projective plane *PG(2,5)*. In this table, each row corresponds to a specific line,

denoted as D_i, where i ranges from 1 to 31. For each line D_i, the table lists the points on that line.

Table 1. The points and lines based on incidence relation

D_1	N_2	N_3	N_{17}	N_{22}	N_{24}	N_{30}
D_2	N_3	N_4	N_{18}	N_{23}	N_{25}	N_{31}
D_3	N_4	N_5	N_{19}	N_{24}	N_{26}	N_1
D_4	N_5	N_6	N_{20}	N_{25}	N_{27}	N_2
D_5	N_6	N_7	N_{21}	N_{26}	N_{28}	N_3
D_6	N_7	N_8	N_{22}	N_{27}	N_{29}	N_4
D_7	N_8	N_9	N_{23}	N_{28}	N_{30}	N_5
D_8	N_9	N_{10}	N_{24}	N_{29}	N_{31}	N_6
D_9	N_{10}	N_{11}	N_{25}	N_{30}	N_1	N_7
D_{10}	N_{11}	N_{12}	N_{26}	N_{31}	N_2	N_8
D_{11}	N_{12}	N_{13}	N_{27}	N_1	N_3	N_9
D_{12}	N_{13}	N_{14}	N_{28}	N_2	N_4	N_{10}
D_{13}	N_{14}	N_{15}	N_{29}	N_3	N_5	N_{11}
D_{14}	N_{15}	N_{16}	N_{30}	N_4	N_6	N_{12}
D_{15}	N_{16}	N_{17}	N_{31}	N_5	N_7	N_{13}
D_{16}	N_{17}	N_{18}	N_1	N_6	N_8	N_{14}
D_{17}	N_{18}	N_{19}	N_2	N_7	N_9	N_{15}
D_{18}	N_{19}	N_{20}	N_3	N_8	N_{10}	N_{16}
D_{19}	N_{20}	N_{21}	N_4	N_9	N_{11}	N_{17}
D_{20}	N_{21}	N_{22}	N_5	N_{10}	N_{12}	N_{18}
D_{21}	N_{22}	N_{23}	N_6	N_{11}	N_{13}	N_{19}
D_{22}	N_{23}	N_{24}	N_7	N_{12}	N_{14}	N_{20}
D_{23}	N_{24}	N_{25}	N_8	N_{13}	N_{15}	N_{21}
D_{24}	N_{25}	N_{26}	N_9	N_{14}	N_{16}	N_{22}
D_{25}	N_{26}	N_{27}	N_{10}	N_{15}	N_{17}	N_{23}
D_{26}	N_{27}	N_{28}	N_{11}	N_{16}	N_{18}	N_{24}
D_{27}	N_{28}	N_{29}	N_{12}	N_{17}	N_{19}	N_{25}
D_{28}	N_{29}	N_{30}	N_{13}	N_{18}	N_{20}	N_{26}
D_{29}	N_{30}	N_{31}	N_{14}	N_{19}	N_{21}	N_{27}
D_{30}	N_{31}	N_1	N_{15}	N_{20}	N_{22}	N_{28}
D_{31}	N_1	N_2	N_{16}	N_{21}	N_{23}	N_{29}

INVESTIGATION OF COMPLETE (10,3)-ARCS BASED ON THE MENELAUS CONFIGURATION IN PG(2,5)

This section presents an algorithm used to construct complete (10,3)-arcs by including the Menelaus configuration and utilizing secant distributions in

PG(2,5).
Two different methods are applied to obtain a total of thirty-two different complete (10,3)-arcs:

> Method 1. → contructs twenty-four different complete (10,3)-arcs
> Method 2. → contructs eight different complete (10,3)-arcs

Each method follows a structured approach, ensuring systematic identification and completion of arcs.

Methodology: Constructing (10,3)-Arcs in PG(2,5)

This section presents an algorithm designed to construct (10,3)-arcs, incorporating the Menelaus configuration and utilizing secant distributions in PG(2,5). The algorithm follows a structured approach, ensuring systematic identification and extension of arcs.

Step 1: Initialization and Projective Plane Definition

- Identify the points and lines of *PG(2,5)* using the irreducible polynomial
$$f(x) = x^3 + 2x^2 + x - 1 \text{ over } GF(5).$$
- Applying this polynomial, determine *31* points and *31* lines in the projective plane (see Table 1).
- Store the identified points and lines in dataset A.

Step 2: Definition of the Menelaus Configuration

- Consider a Menelaus configuration M in PG(2,5), consisting of six points: $M = \{A_1, A_2, A_3, B_1, B_2, B_3 \}$.
- *M forms an incomplete (6,3)-arc in PG(2,5).*

Step 3: Determination of Remaining Points

- Identify 13 points that do not lie on the lines of M.
- Classify these 13 points into three categories based on their secant line properties to Menalaus configuration M in PG(2,5):

1. Category 1: Six points have
   - One 0-secant line
   - Four 1-secant lines
   - One 2-secant line
2. Category 2: Four points have
   - Six 1-secant lines
3. Category 3: Three points have
   - Two 0-secant lines

- o   Two 1-secant lines
- o   Two 2-secant lines

Step 4: Construction of the Triangle

- Category 3 points define a triangle in PG(2,5):

$$C_1 = A_1 B_1 \cap A_2 B_2,$$
$$C_2 = A_1 B_1 \cap A_3 B_3,$$
$$C_3 = A_2 B_2 \cap A_3 B_3.$$

  where $\sigma_2(C_j) = 2, \sigma_1(C_j) = 2, \sigma_0(C_j) = 2, j = 1, 2, 3.$

- Each edge of this triangle intersects the Menelaus configuration at two points.
- The triangle $C_1 C_2 C_3$ such that the points C_1, C_2, C_3 of this triangle are with 2 -index out of M.

Step 5: First Method – Constructing complete (10,3)-Arcs using $\sigma_2(C_j)$ =2, j=1,2,3

Step 5.1: Constructing the (7,3)-Arc

- Select one of the Category 3 points and add it to the (6,3)-arc, then an incomplete (7,3)-arc is obtained as $M \cup \{C_j\}, j = 1, 2, 3.$
- The remaining six points consist of:
  - o   Two in Category 1
  - o   Four in Category 2

Step 5.2: Constructing the (8,3)-Arc

- Identify two of Category 1 points $D_k, k = 1, 2, \ldots 6$ on a triangle edge not adjacent to C_1 where $\sigma_2(D_k) = 1, \sigma_1(D_k) = 4, \sigma_0(D_k) = 1 \; k = 1, 2, \ldots 6.$
- Select one and add it to the (7,3)-arc, then an incomplete (8,3)-arc is obtained.
- The remaining four points consist of Category 2.

Step 5.3: Constructing the (9,3)-Arc

- The remaining four Category 2 points (E_1, E_2, E_3, E_4) form a quadrangle where $\sigma_1(E_l) = 6, l = 1, 2, 3, 4.$
- The diagonal points of this quadrangle define the triangle $C_1 C_2 C_3$.

- Select two points on the quadrangle edge that does not pass through C_1 and add them to the (8,3)-arc, then a complete (10,3)-arc is obtained.

Step 6: Second Method – Constructing complete (10,3)-Arcs using $\sigma_2(D_k)=1$, k=1,2,…6

- Each edge of the triangle $C_1C_2C_3$ contains two Category 1 points.
- Since these edges are 2-secant lines, selecting one point per edge and adding it to the (6,3)-arc results in an incomplete (9,3)-arc.
- The one remaining point is in Category 2. And if this one remaining Category 2 point of index one is added to the (9,3)-arc, then a complete (10,3)-arc is obtained.

Algorithm Implementation

We present the following algorithm, implemented in C#, designed to identify complete *(k,3)-arcs* within *PG(2,5):*

$A \leftarrow Read(Excel\ File)$
$B \leftarrow Read(Text\ File)$
$C \leftarrow A$
while s(C)>0
  $B_i \leftarrow input(b), \{b|b \in C, b \notin B, i = s(B) + 1\}$
  j=1
  while $j \leq s(B)$
    for k=(j+1) to s(B)
      $m \leftarrow$ *the index of row on B_j, B_k*
      $D \leftarrow A_{mn}; \{A_{mn}|A_{mn} \neq B_j, A_{mn} \neq B_k, n = 1,\ldots,10\}$
      Remove a from A; $\{a|a \in A, a \in D\}$
      $C \leftarrow c; \{c|c \in A, c \notin C\}$
    end for
    j=j+1
  end while
end while

Theorem 2. Menelaus configuration determines an incomplete (6,3)-arc in PG(2,5).
Proof. Let M= $\{A_1, A_2, A_3, B_1, B_2, B_3\}$ be any Menelaus configuration in PG(2,5). M contains six lines and six points. From Theorem 1, since no four points in the Menelaus configuration are collinear, the set of these points forms a (6,3)-arc. From Definition 5, This (6,3)-arc is not complete.

Now, if the given algorithm is applied to the points of the incomplete (6,3)-arc determined by Menelaus configuration to find (k,3)-arcs, then there are thirteen remaining points.

Theorem 3. There are thirty-two different complete (10,3) −arcs containing a Menalaus configuration in *PG(2,5).*

Proof. Let M be a Menelaus configuration. From Theorem 2, M is an incomplete (6,3)-arc in PG(2,5). If the given algorithm is applied to M to find (k,3)-arcs, there are thirteen remaining points which are classified into three categories based on their secant lines. Nine of these thirteen remaining points are 2-index points. Among them, three points C_j have $\sigma_2(C_j) = 2, j = 1, 2, 3,$ and six points D_k have $\sigma_2(D_k) = 1, k = 1,2,\dots,6$. When the Menelaus configuration and these categories are examined, it is observed that the points C_1, C_2, C_3 in Category 3 have two 2-secant lines and form a triangle $C_1 C_2 C_3$ as $A_1 B_1 \cap A_2 B_2 = C_1, A_1 B_1 \cap A_3 B_3 = C_2, A_2 B_2 \cap A_3 B_3 = C_3$.
And also, the remaining points $D_k, k = 1, 2, \dots, 6$ are located two by two on the edges of this triangle such that $D_1, D_5 \circ C_1 C_3, D_2, D_6 \circ C_2 C_3, D_3, D_4 \circ C_1 C_2$.

i) If one of these points is selected as C_1 and added to *M,* and this algorithm is applied, then an incomplete (7,3)-arc M_1 is obtained as $M \cup \{C_1\} = \{A_1, A_2, A_3, B_1, B_2, B_3, C_1\}$. After C_1 is added, two points remain to be added to (7,3)-arc from the remaining points $D_k, k = 1, 2, \dots, 6$. Suppose that two remaining points D_2, D_6 are located on the edge $C_2 C_3$ not on the point C_1 of the triangle $C_1 C_2 C_3$. If one of these points is added to M_1, and the algorithm is applied, then an incomplete (8,3)-arc M_2 is obtained as $M \cup \{C_1, D_2\} = \{A_1, A_2, A_3, B_1, B_2, B_3, C_1, D_2\}$. When the algorithm is applied M_2, then four remaining points E_1, E_2, E_3, E_4 in Category 2 to can be added M_2 remain. Any three of them E_1, E_2, E_3, E_4 are not collinear, and each of them has six 1-secant lines. So, these points form a quadrangle $E_1 E_2 E_3 E_4$, and the diagonal points of this quadrangle $E_1 E_2 E_3 E_4$ are C_1, C_2, C_3. If two points on the edge of the quadrangle $E_1 E_2 E_3 E_4$ that does not pass through C_1 are added to M_2, then a (10,3)-arc is obtained as $M_3 = M_2 \cup \{E_1, E_2\}$. Since there isn't any remaining point that can be added to M_3, M_3 is a complete (10,3)-arc.
Since there are three different choices for C_j, two different choices for D_k, and four different choices for E_l, applying all possible selections within this method results in twenty-four different complete (10,3)-arcs.
ii) Consider again the triangle $C_1 C_2 C_3$. Since these edge lines of the triangle $C_1 C_2 C_3$ are 2-secant lines, if one of the two points D_k on each edge is selected and added to the incomplete (6,3)-arc formed by the Menelaus configuration, an incomplete (9,3)-arc is obtained such as $M \cup \{D_1, D_2, D_4\}$. If the algorithm is applied, one point belonging to Category 2 remains. If this point is added to the incomplete (9,3)-arc, a complete (10,3)-arc is obtained. Applying all

possible selections of the points D_k within Category 1, eight different complete (10,3)-arcs are obtained.

So from i) and ii), there are thirty-two different complete *(10,3)-arcs* including Menelaus configuration in *PG(2,5)*.

Let M be Menalaus configuration $\{N_2, N_3, N_5, N_6, N_{21}, N_{22}\}$. By applying this algorithm to M it is seen that $M = \{N_2, N_3, N_5, N_6, N_{21}, N_{22}\}$ is *(6,3)-arc* but an incomplete arc. In this projective plane, the points on the lines spanned by *(6,3)-arc* are deleted in *PG(2,5)*, then N_1, N_4, N_8, N_9, N_{11}, N_{13}, N_{14}, $N_{15}, N_{16}, N_{19}, N_{23}, N_{29}, N_{31}$ points are remained. Since six lines pass through each of these points in PG(2,5), these points can be classified into three categories based on their secant line properties. In Table 2, 0-secant, 1−secant and 2−secant lines of the Menalaus configuration passing through the remaining points out of (6, 3)−arc are given in PG(2,5).

Table 2. The remaining points and the secant lines of the Menalaus configuration

Category Type	Point	0-secant	1-secant	2-secant
Category 1	N_1	D_9	$D_3, D_{11}, D_{16}, D_{30}$	D_{31}
	N_{13}	D_{28}	$D_{11}, D_{12}, D_{15}, D_{23}$	D_{21}
	N_{14}	D_{22}	$D_{12}, D_{16}, D_{24}, D_{29}$	D_{13}
	N_{15}	D_{25}	$D_{14}, D_{17}, D_{23}, D_{30}$	D_{13}
	N_{16}	D_{26}	$D_{14}, D_{15}, D_{18}, D_{24}$	D_{31}
	N_{19}	D_{27}	$D_3, D_{17}, D_{18}, D_{29}$	D_{21}
Category 2	N_4		$D_2, D_3, D_6, D_{12}, D_{14}, D_{19}$	
	N_8		$D_6, D_7, D_{10}, D_{16}, D_{18}, D_{23}$	
	N_9		$D_7, D_8, D_{11}, D_{17}, D_{19}, D_{24}$	
	N_{31}		$D_2, D_8, D_{10}, D_{15}, D_{29}, D_{30}$	
Category 3	N_{11}	D_9, D_{26}	D_{10}, D_{19}	D_{13}, D_{21}
	N_{23}	D_{22}, D_{25}	D_2, D_7	D_{21}, D_{31}
	N_{29}	D_{27}, D_{28}	D_6, D_8	D_{13}, D_{31}

When these categories are examined, it is observed that the points in Category 3 have two 2-secant lines and form a triangle $N_{11} N_{23} N_{29}$. The edges of this triangle intersect the Menalaus configuration at two points.

Example 1.
Let M be Menalaus configuration $\{N_2, N_3, N_5, N_6, N_{21}, N_{22}\}$. By applying this algorithm to M it is seen that $M = \{N_2, N_3, N_5, N_6, N_{21}, N_{22}\}$ is *(6,3)-arc* but incomplete arc. In this projective plane, the points on the lines spanned by *(6,3)-arc* are deleted in $PG(2,5)$, then $N_1, N_4,$ $N_8,$ $N_9, N_{11}, N_{13},$ $N_{14},$ $N_{15}, N_{16}, N_{19}, N_{23}, N_{29}, N_{31}$ points are remained. Since six lines pass through each of these points in $PG(2,5)$, these points can be classified into three categories based on their secant line properties. In Table 2, 0-secant, 1−secant and 2−secant lines of the Menalaus configuration passing through the remaining points out of $(6, 3)$−arc are given in $PG(2,5)$.

Table 2. The remaining points and the secant lines of the Menalaus configuration

Category Type	Point	0-secant	1-secant	2-secant
Category 1	N_1	D_9	$D_3, D_{11}, D_{16}, D_{30}$	D_{31}
	N_{13}	D_{28}	$D_{11}, D_{12}, D_{15}, D_{23}$	D_{21}
	N_{14}	D_{22}	$D_{12}, D_{16}, D_{24}, D_{29}$	D_{13}
	N_{15}	D_{25}	$D_{14}, D_{17}, D_{23}, D_{30}$	D_{13}
	N_{16}	D_{26}	$D_{14}, D_{15}, D_{18}, D_{24}$	D_{31}
	N_{19}	D_{27}	$D_3, D_{17}, D_{18}, D_{29}$	D_{21}
Category 2	N_4		$D_2, D_3, D_6, D_{12}, D_{14}, D_{19}$	
	N_8		$D_6, D_7, D_{10}, D_{16}, D_{18}, D_{23}$	
	N_9		$D_7, D_8, D_{11}, D_{17}, D_{19}, D_{24}$	
	N_{31}		$D_2, D_8, D_{10}, D_{15}, D_{29}, D_{30}$	
Category 3	N_{11}	D_9, D_{26}	D_{10}, D_{19}	D_{13}, D_{21}
	N_{23}	D_{22}, D_{25}	D_2, D_7	D_{21}, D_{31}
	N_{29}	D_{27}, D_{28}	D_6, D_8	D_{13}, D_{31}

When these categories are examined, it is observed that the points in Category 3 have two 2-secant lines and form a triangle $N_{11}N_{23}N_{29}$. The edges of this triangle intersect the Menelaus configuration at two points.
According to Method 1, if the point N_{11} is selected and added to the incomplete (6,3)-arc $M = \{N_2, N_3, N_5, N_6, N_{21}, N_{22}\}$ formed by the Menelaus configuration, and then the algorithm is applied, an incomplete (7,3)-arc is obtained as $M_1 = \{N_2, N_3, N_5, N_6, N_{11}, N_{21}, N_{22}\}$. Accordingly, six different points $N_1, N_4, N_8, N_9, N_{16},$ and N_{31} remain, with two belonging to Category 1 and four to Category 2. These two remaining points, N_1 and N_{16}, lie on the edge opposite $N_{11},$ and the line they span is a 2-secant of the Menelaus

configuration. If the point N_1 is added to the incomplete (7,3)-arc M_1, an incomplete (8,3) arc is obtained as $M_2 = \{N_1, N_2, N_3, N_5, N_6, N_{11}, N_{21}, N_{22}\}$, and after applying the algorithm, four points N_4, N_8, N_9, and N_{31} remain, none of which are collinear, and these points correspond to the vertices of a quadrilateral such that its edges intersect the Menelaus configuration at one point. Also, the triangle $N_{11}N_{23}N_{29}$ forms the diagonal triangle of this quadrilateral $N_4N_8N_9N_{31}$. There are six 1-secant lines passing through these four points N_4, N_8, N_9, N_{31}. If two points N_4, N_8 on the edge of the quadrangle $N_4N_8N_9N_{31}$ that does not pass through N_{11} are added to M_2, then a (10,3)-arc is obtained as $M_3 = M_2 \cup \{N_4, N_8\} = \{N_1, N_2, N_3, N_4, N_5, N_6, N_8, N_{11}, N_{21}, N_{22}\}$. After the algorithm is applied, M_3 is a complete (10,3)-arc as no further point can be added to it.

The process continues according to Method 2 to obtain a (10,3)-arc. Consider again the triangle $N_{11}N_{23}N_{29}$. If the points N_1, N_{14}, and N_{19} are selected, one from each edge of this triangle, and added to M, an incomplete (9,3)-arc is obtained as $M_1 = M \cup \{N_1, N_{14}, N_{19}\} = \{N_1, N_2, N_3, N_5, N_6, N_{14}, N_{19}, N_{21}, N_{22}\}$. Then, after the algorithm is applied, one point, N_9, remains and can be added to M_1, belonging to Category 2. By adding N_9, a complete (10,3)-arc is obtained as $M_2 = M_1 \cup \{N_9\} = \{N_1, N_2, N_3, N_5, N_6, N_9, N_{14}, N_{19}, N_{21}, N_{22}\}$.

All complete (10,3)-arcs obtained based on all possible configurations of the remaining points using Method 1 and Method 2 are presented in Table 3, resulting in thirty-two distinct complete (10,3)-arcs.

Table 3. Complete (10,3)-arcs

Completion of (6,3)-arc	Complete (10,3)-arcs
M $\cup \{N_1, N_4, N_8, N_{11}\}$	$\{N_1, N_2, N_3, N_4, N_5, N_6, N_8, N_{11}, N_{21}, N_{22}\}$.
M $\cup \{N_1, N_4, N_{11}, N_{31}\}$	$\{N_1, N_2, N_3, N_4, N_5, N_6, N_{11}, N_{21}, N_{22}, N_{31}\}$
M $\cup \{N_1, N_4, N_{13}, N_{15}\}$	$\{N_1, N_2, N_3, N_4, N_5, N_6, N_{13}, N_{15}, N_{21}, N_{22}\}$
M $\cup \{N_1, N_8, N_9, N_{11}\}$	$\{N_{41}, N_2, N_3, N_5, N_6, N_8, N_9, N_{11}, N_{21}, N_{22}\}$
M $\cup \{N_1, N_8, N_{15}, N_{19}\}$	$\{N_1, N_2, N_3, N_5, N_6, N_8, N_{15}, N_{19}, N_{21}, N_{22}\}$
M $\cup \{N_1, N_9, N_{11}, N_{31}\}$	$\{N_1, N_2, N_3, N_5, N_6, N_9, N_{11}, N_{21}, N_{22}, N_{31}\}$
M $\cup \{N_1, N_9, N_{14}, N_{19}\}$	$\{N_1, N_2, N_3, N_5, N_6, N_9, N_{14}, N_{19}, N_{21}, N_{22}\}$
M $\cup \{N_1, N_{13}, N_{14}, N_{31}\}$	$\{N_1, N_2, N_3, N_5, N_6, N_{13}, N_{14}, N_{21}, N_{22}, N_{31}\}$
M $\cup \{N_4, N_8, N_{11}, N_{16}\}$	$\{N_2, N_3, N_4, N_5, N_6, N_8, N_{11}, N_{16}, N_{21}, N_{22}\}$
M $\cup \{N_4, N_8, N_{14}, N_{23}\}$	$\{N_2, N_3, N_4, N_5, N_6, N_8, N_{14}, N_{21}, N_{22}, N_{23}\}$
M $\cup \{N_4, N_8, N_{15}, N_{23}\}$	$\{N_2, N_3, N_4, N_5, N_6, N_8, N_{15}, N_{21}, N_{22}, N_{23}\}$
M $\cup \{N_4, N_9, N_{13}, N_{29}\}$	$\{N_2, N_3, N_4, N_5, N_6, N_9, N_{13}, N_{21}, N_{22}, N_{29}\}$
M $\cup \{N_4, N_9, N_{14}, N_{23}\}$	$\{N_2, N_3, N_4, N_5, N_6, N_9, N_{14}, N_{21}, N_{22}, N_{23}\}$
M $\cup \{N_4, N_9, N_{15}, N_{23}\}$	$\{N_2, N_3, N_4, N_5, N_6, N_9, N_{15}, N_{21}, N_{22}, N_{23}\}$
M $\cup \{N_4, N_9, N_{19}, N_{29}\}$	$\{N_2, N_3, N_4, N_5, N_6, N_9, N_{19}, N_{21}, N_{22}, N_{29}\}$

$M \cup \{N_4, N_{11}, N_{16}, N_{31}\}$	$\{N_2, N_3, N_4, N_5, N_6, N_{11}, N_{16}, N_{21}, N_{22}, N_{31}\}$
$M \cup \{N_4, N_{13}, N_{29}, N_{31}\}$	$\{N_2, N_3, N_4, N_5, N_6, N_{13}, N_{21}, N_{22}, N_{29}, N_{31}\}$
$M \cup \{N_4, N_{14}, N_{16}, N_{19}\}$	$\{N_2, N_3, N_4, N_5, N_6, N_{14}, N_{16}, N_{19}, N_{21}, N_{22}\}$
$M \cup \{N_4, N_{19}, N_{29}, N_{31}\}$	$\{N_2, N_3, N_4, N_5, N_6, N_{19}, N_{21}, N_{22}, N_{29}, N_{31}\}$
$M \cup \{N_8, N_9, N_{11}, N_{16}\}$	$\{N_2, N_3, N_5, N_6, N_8, N_9, N_{11}, N_{16}, N_{21}, N_{22}\}$
$M \cup \{N_8, N_9, N_{13}, N_{29}\}$	$\{N_2, N_3, N_5, N_6, N_8, N_9, N_{13}, N_{21}, N_{22}, N_{29}\}$
$M \cup \{N_8, N_9, N_{19}, N_{29}\}$	$\{N_2, N_3, N_5, N_6, N_8, N_9, N_{19}, N_{21}, N_{22}, N_{29}\}$
$M \cup \{N_8, N_{13}, N_{14}, N_{16}\}$	$\{N_2, N_3, N_5, N_6, N_8, N_{13}, N_{14}, N_{16}, N_{21}, N_{22}\}$
$M \cup \{N_8, N_{13}, N_{29}, N_{31}\}$	$\{N_2, N_3, N_5, N_6, N_8, N_{13}, N_{21}, N_{22}, N_{29}, N_{31}\}$
$M \cup \{N_8, N_{14}, N_{23}, N_{31}\}$	$\{N_2, N_3, N_5, N_6, N_8, N_{14}, N_{21}, N_{22}, N_{23}, N_{31}\}$
$M \cup \{N_8, N_{15}, N_{23}, N_{31}\}$	$\{N_2, N_3, N_5, N_6, N_8, N_{15}, N_{21}, N_{22}, N_{23}, N_{31}\}$
$M \cup \{N_8, N_{19}, N_{29}, N_{31}\}$	$\{N_2, N_3, N_5, N_6, N_8, N_{19}, N_{21}, N_{22}, N_{29}, N_{31}\}$
$M \cup \{N_9, N_{11}, N_{16}, N_{31}\}$	$\{N_2, N_3, N_5, N_6, N_9, N_{11}, N_{16}, N_{21}, N_{22}, N_{31}\}$
$M \cup \{N_9, N_{13}, N_{15}, N_{16}\}$	$\{N_2, N_3, N_5, N_6, N_9, N_{13}, N_{15}, N_{16}, N_{21}, N_{22}\}$
$M \cup \{N_9, N_{14}, N_{23}, N_{31}\}$	$\{N_2, N_3, N_5, N_6, N_9, N_{14}, N_{21}, N_{22}, N_{23}, N_{31}\}$
$M \cup \{N_9, N_{15}, N_{23}, N_{31}\}$	$\{N_2, N_3, N_5, N_6, N_9, N_{15}, N_{21}, N_{22}, N_{23}, N_{31}\}$
$M \cup \{N_{15}, N_{16}, N_{19}, N_{31}\}$	$\{N_2, N_3, N_5, N_6, N_{15}, N_{16}, N_{19}, N_{21}, N_{22}, N_{31}\}$

CONCLUSION

In this study, we have systematically constructed and analyzed complete *(10,3)*-arcs in the projective plane *PG(2,5),* each containing a Menelaus configuration. By implementing a structured algorithm in *C#*, we identified and classified the remaining points outside the Menelaus configuration based on their secant properties, particularly focusing on the distribution of *0-secant, 1-secant,* and *2-secant* lines. Through this classification, we introduced two distinct methods that together yielded a total of thirty-two different complete *(10,3)*-arcs.

The first method focused on the triangle formed by Category 3 points with two *2*-secant lines, resulting in twenty-four distinct complete *(10,3)*-arcs. The second method utilized the structured placement of index-*2* points on the edges of this triangle. By selecting one such point per edge and then adding the remaining point in Category 2, eight complete *(10,3)*-arcs were obtained. As a result, a total of thirty-two different complete *(10,3)*-arcs containing a Menelaus configuration are identified in *PG(2,5)*.

This work contributes to the structural understanding of arcs derived from classical configurations in finite projective geometry and offers a computational approach to their classification.

REFERENCES

[1] J.W.P. Hirschfeld and J.A. Thas, "General Galois Geometries," *Springer Monographs in Mathematics*. Springer- Verlag London, 2016.

[2] A. Bayar, Z. Akca, E. Altintas, and S. Ekmekci, S. "On the complete arcs containing the quadrangles constructing the Fano planes of the left near field plane of order 9," *New Trend Math. Sci.*, 4(4), 266-266, 2016. http://dx.doi.org/10.20852/ntmsci.2016.113

[3] S. Ekmekci, A. Bayar, E. Altintas, and Z. Akca, "On the Complete (k,2)- Arcs of the Hall Plane of Order 9," *IJARCSSE*, 6 (10), 282-288, 2016. ISSN: 2277 128X.

[4] Z. Akca, S. Ekmekci, and A. Bayar, "On Fano Configurations of the Left Hall Plane of order 9," *Konuralp J. Math.*, 4 (2), 116-123, 2016.

[5] Z. Akca, and A. Altıntas, "A Note on Fano Configurations in the Projective Space PG(5,2)," *Konuralp J. Math.*, 9(1), 190-192, 2021.

[6] Z. Akca, "A numerical computation of (k, 3)-arcs in the left semifield plane order 9*", Int. Electron. J. Geom.*, 4(2), 13-21, 2011.

[7] Z. Akca, and I. Günaltılı, I. "On the (k, 3)- arcs of CPG (2,25,5)," *Anadolu Univ J Sci Technol J Theor Sci,* 1(0), 21-27, 2012.

[8] E. Altıntas, and A. Bayar, "Complete (k,2)-Arcs in the Projective Plane Order 5," *HSJG*, 5(1), 11-14, 2023. e-ISSN 2687-4261.

[9] E. Altıntaş Kahriman, A. Bayar, "On (k,3)-arcs derived by Ceva configurations in PG(2,5)," *Journal of Scientific Reports-A*, 059, 10–18, 2024, doi: 10.59313/jsr-a.1559383.

[11] V. Danos, and L. Regnier, "The structure of multiplicatives," *Arch Math Logic*, 28, 181-203, 1989. https://doi.org/10.1007/BF01622878
[12] J. Benitez, "A unified proof of Ceva and Menelaus' theorems using projective geometry," *JGG*, 11(1):39–44, 2007. ISSN 1433-8157
[13] V. Nicolae, "On The Ceva's And Menelaus's Theorems." *Rom. J. Phys.,* [S.l.], v. 5, n. 2, p. 43-50, 2020. ISSN 2537-5229.
[14] B.K. Funk, "Ceva and Menelaus in projective geometry," University of Louisuille, 42 p, 2008.
[15] S. Çiftçi, R. Kaya, and J.C. Ferrar, "On Menelaus and Ceva 6-figures in Moufang projective planes," *Geom. Dedicata*, vol. 19, no. 3, pp. 295–296, 1985.
[16] A. Bayar, and S. Ekmekçi, "On the Menelaus and Ceva 6-figures in the fibered projective planes," *Abstr. Appl. Anal.*,1-5, 2014. 10.1155/2014/803173
[17] Z. Akça, A. Bayar, and S. Ekmekçi, "On the intuitionistic fuzzy projective Menelaus and Ceva's conditions," *Commun. Fac. Sci. Univ. Ank. Ser. A1 Math. Stat.,* 69(1), 891-899, 2020. https://doi.org/10.31801/cfsuasmas.567753.
[18] J.W.P. Hirschfeld, and J.A. Thas, "General Galois Geometries," *The Charendon Press*, Oxford, 1991.

[19] J.W.P. Hirschfeld, and J.F. Voloch, "Group-arcs of prime order on cubic curves," *Finite Geometry and Combinatorics*, 191, 177-185, 2015.

[20] J.W.P. Hirschfeld, and E.V.D. Pichanick "Bounded for arcs of arbitrary degree in finite Desarguesian Planes" *J Comb Des.,* 24(4), 184-196, 2016.

[21] B.A. Qassim, "The construction for the arcs (8,4)-from the two arcs (7,4)-in PG (2,q), q=5," *J. Phys. Conf. Ser.,* 1664012039, 2020.

The Catechin and Biological Activity

Muhammed Kerim ÇALAPVERDİ[1]

Hülya ÇELİK[2*]

1 Ağrı İbrahim Çeçen University, Faculty of Pharmacy, Ağrı, Turkey kerimclpvrd@gmail.com
2 Ağrı İbrahim Çeçen University, Faculty of Pharmacy/ Department of Basic Pharmaceutical Sciences/ Department of Basic Pharmacy Sciences04100 Ağrı/Türkiye ORCID:0000-0003-0805-0523
Corresponding author: Hülya ÇELİK hycelik@agri.edu.tr

ABSTRACT

Catechins have an important role in supporting our health as a natural type of flavonoid. These compounds, which are especially abundant in sources such as green tea, have a wide range of positive health effects and are therefore of interest to researchers. Research has shown that catechins exhibit a variety of biological activities and may be a potential solution to difficult-to-treat diseases. Catechins are known to support many biological activities such as antiallergic, antiangiogenesis, antimicrobial, antifungal, antiviral, antimtagenic, antiobesity, antidiabetes, antioxidant, antiprotective, and anticancer. Furthermore, research shows that catechins provide positive effects on COPD, cholesterol, and cardiovascular health. Catechins remain important as a potential health resource that has been studied and is still being studied. Studies to better understand the health effects of these valuable compounds and expand their uses may offer important information that may provide more health benefits in the future.

Key words: Catechin, Biological activity, Flavonoid

INTRODUCTION

What are catechins and in which foods are they found?

Today, old natural treatments are as important as clinical treatment. However, the benefits of herbal products are also a matter of curiosity and research by experts about the healing properties of the chemical groups in these products. Catechins are also one of the components that experts focus on the benefit of and are the subject of great scrutiny.

Catechins are flavanols in the group of polyphenols. Catechins are found in tea, wine, chocolate, fruit and soft drinks. Due to the 2,3 double bonds contained in these flavonoids, catechins are studied in 8 different stereoisomerides (1)

The most important of these are catechin and epicatechin. (+) The catechin carries a betahydroxyl (OH) group in the C ring, while the (-) epicatechin carries an alpha OH group in the C ring. Catechins are found in the structure of many foods, and we obtain these flavanols from food. The table below gives some foods and the amount of catechins they contain. (2)

Table 1. Presence of catechins in foods (Musial et al.2020) (3)

Food	Catechin Content
Apple	17 mg/kg K+ 129 mg/kg EK
Chocolate (black)	610 mg/kg K+ EK
Chocolate (milk)	159 mg/kg K+ EK
Cocoa	78 mg/L K+ 132 mg/L EK
Grape	1892 mg/kg K+ 988 mg/kg EC+353 mg/kg ECG
Kiwi	4.5 mg/kg K+ EK
Strawberry	10-70 mg/kg K+ 1 mg/kg EK
Tea (black)	20 mg/L K+ 37 mg/L EK+ 73 mg/L ECG+42 mg/L EGK+ 128 mg/L EGKG
Tea (green)	21 mg/L K+ 98 mg/L EK+ 90 mg/L ECG+411 mg/L EGK+ 444 mg/L EGKG
Wine (red)	27-96 mg/L
Beer	0.1-5 mg/L

The richest food source in terms of catechins is tea. Catechins are the main bioactive components in tea leaves. (25-35% of dry weight) A cup of green tea contains up to 200 mg of catechins. Tea, which has a very high catechin ratio (especially green tea, this rate is much higher), has become an important food for alternative medicine and modern medicine due to this feature. (2)

Tea

Figure 1. Green Tea(Wikipedia.org)

History of Tea

Tea (Camelliasins) is a green leafy plant belonging to the Theaceae family. It grows in humid climates. About 5000 years ago, he was discovered by the Chinese Emperor ShenNung (Legendary Red Emperor) by falling into boiling water by chance, and his taste, color and smell were liked. Since then, tea has spread all over the world. It is produced in about 30 countries. In our country, tea started to be produced in 1888. (2)

 The Medicinal Importance of Tea

Black and green teas, which are similar beverages in terms of content, show their antioxidant effects with the different substances they contain. Green tea contains a large amount of polyphenols from the flavonoid group. In addition, the presence of catechins from the polyphenol group and epigallocatechingallate (EGCG) from catechins is also high. In addition, epigallocatechin (EGC), epicatechiningallate (ECG), epicatechin (EC), catechin (C), gallocatechin (GC) and gallocatechingallate (GCG) are also available in different amounts. The most important catechins of black tea are theaflavins (TF) and thearubigins (TB), which also give black tea its color and astringent aroma. The ratios of the ingredients found in black and green tea are presented in the table below (1)

Table 2. Proportions Of Components Found İn A Cup Of Black And Green Tea (4)

COMPONENT	GREEN TEA (1 CUP)	BLACK TEA (1 CUP)
CATECHINS	60-125 MG	30-60 MG
THEAFLAVINS	-	3-6 MG
CAFFEINE	20-50 MG	30-60MG
L-THEANINE	20-40 MG	20-40 MG

Table 3. Ratios Of Catechin Isomers İn Tea Mg/G (4)

COMPONENT	GREEN TEA	BLACK TEA	OOLONG TEA
EPICCATECHIN	6,6	4	1.75
EPICATECIN GALLAT	5,34	1.19	3,58
EPIGALLOCATECHIN	36,5	1	7
EPIGALLOCATECHIN GALLLATE	18,1	1	9
GALLOCATECHIN GALLATE	0,2	-	-
GALLO CATECHIN	2	0,4	-
GALLIC ACID	0,7	2,7	0,5

Studies have shown that tea has protective effects against arthritis, antiviral and anti-inflammatory diseases, especially various types of cancer such as coronary heart diseases (CHD), stroke, cardiovascular diseases (CVD), hypertension (HT), esophagus, stomach, colorectal, lung and prostate, and regulating bone density for all age groups. It is stated that both green and black tea are an antioxidant drink due to the polyphenolic compounds they contain and provide their protective effect from chronic diseases in this way. The antioxidant capacity of flavonoids may enhance endothelial function by reducing oxidative stress. Increased endothelial function affects vasomotor tone, platelet activity, leukocyte adhesion and vascular smooth muscle cells. Studies on humans show that the flavonoids in black tea increase coronary circulation and reduce low-density lipoprotein (LDL) cholesterol by 11.1%. Catechins appear to increase free radical activity in DNA mutations at an early stage of cancer pathogenesis. According to the results of in vitro animal studies, antioxidants were found to be responsible for the anti-inflammatory response. It is stated that the catechins in green tea and the polyphenols in black tea prevent the formation of cancer, have an anti-inflammatory effect and inhibit tumor formation. (1)
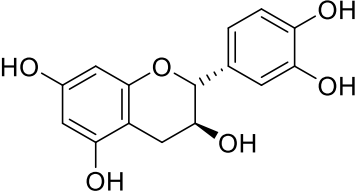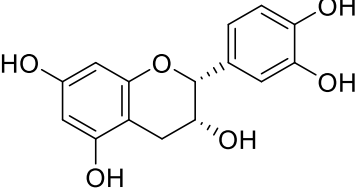
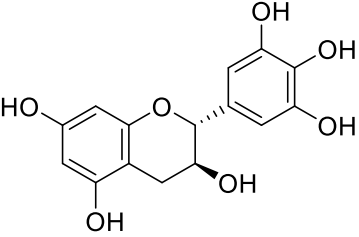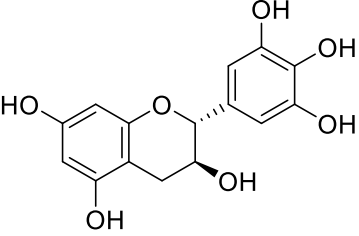## 1.5. Structure and characteristics of the catechin

Catechin was identified in 1803 by a scientist named Davy, and keteschin species, which were first detected in tea, are used in many areas. The crystal
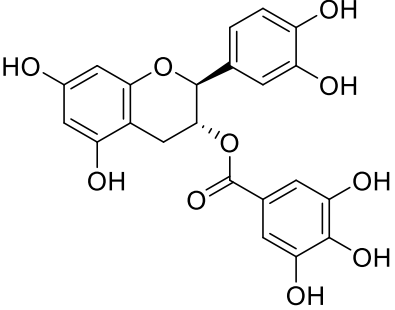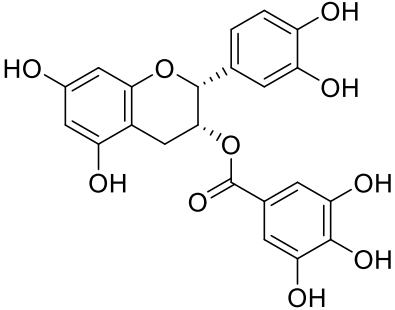
structure of the catechin is in the form of fine needles and its melting point is 212-214 C. Catechin dissolves easily in alcohol and acetone. It is in the form of a catechin C15H14O6 formula, which is a type of flavanol, natural phenol and antioxidant.it consists of 8 different isomers in the family of catechins (flavan-3-ol). These are the following compounds. (5)

(+) catechin (K), (-) epicatechin (EK), (+) gallocatechin (GK), (-) epigallocatechin (EGK), (+) catechiningallate (KG), (-) epicatechiningallate (ECG), (+) gallocatechingallate (GKG), (-) epigallocatechingallate (EGKG)
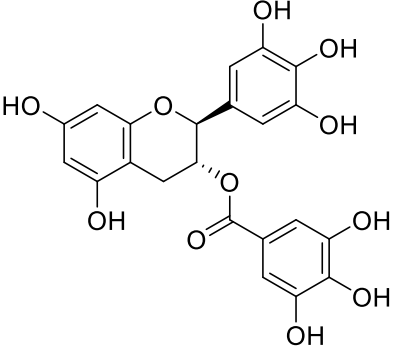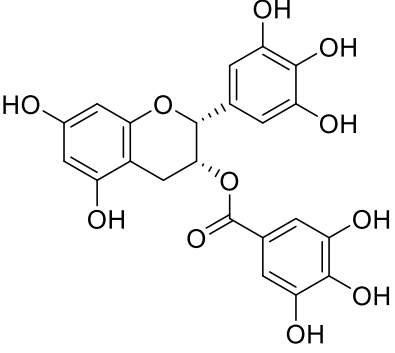
Table 4.Types of catechins, chemical formulas

Compound Name	Chemical Structure
(+) catechin (K)	
(-) epicatechin (EK)	

(+) gallocatechin (GK)	
(-) epigallocatechin	

(+) catechiningallate (KG)	
(-) epicatechiningallate (ECG)	

(+) gallocatechingalate (GKG)	
(-) epigallocatechingallate (EGKG)	

Due to the various qualities of catechins that are beneficial to one's health, it is recommended that food items, especially those containing catechins, be included in one's diet on a daily basis. It is believed that the catechin group has the most significant effect due to its chemopreventive, anti-inflammatory and antioxidant properties.

Catechins act as powerful antioxidants by neutralizing reactive oxygen species, limiting the formation of free radicals, and inhibiting lipid peroxidation. These functions are pivotal for their role in plant protection. Studies highlight that the antioxidant properties of green tea catechins, along with their notable ability to reduce the prevalence of modern civilization-related illnesses, are significantly influenced by the structural elements in their molecules, particularly the hydroxyl group count. Furthermore, research indicates that consuming green tea might contribute to a lower risk of developing various cancers, such as those affecting the esophagus, lungs, prostate, stomach, breasts, pancreas, intestines, and bladder (3).

Many studies have been conducted and continue to be conducted to demonstrate the beneficial effects of catechins on health. These; Anticarcinogen, Antitumorigenic, Antimutagenic, Chemopreventative, Antiproliferative, Anti-inflammatory, Antioxidant, Antidiabetic, Antiallergic, Antihypertensive, Antiplatelet, Antiobesity, Hypocholesterolemic, Neuroprotective effects. (1)

With these studies, catechins have the ability to create the above indications from a medical point of view. After the catechin is absorbed, it reaches the target tissues and shows anticancer activity. It fights against cancer cells by providing the opposite effect at all stages of cancer formation (proliferation, transformation, inflammation, apoptosis, metastasis and occupation stages). It shrinks the tumor. Green tea has potential benefits in the prevention of metabolic syndrome thanks to the catechins in it. It lowers cholesterol. Adjusts blood pressure and blood sugar. Studies have shown that green tea or nutritional supplements containing catechins (EGCG) are beneficial in weight management, blood sugar control and reducing the risk of cardiovascular diseases. It achieves this by increasing fat burning in the body. Increased fat burning reduces adipose tissue. Thanks to the reduced adipose tissue, the risk of obesity, type 2 diabetes, cardiovascular diseases and metabolic syndrome is also reduced. Green tea strengthens blood vessels thanks to the flavonoids in it. Prevents high blood pressure. Catechins also provide relaxation and calming in the person with their sedative effects. Again, today it is

recommended to be used to increase immunity and fight colds. In slimming diets, the fat-burning effect of catechin has been proven. Thanks to its blood sugar control, it also provides appetite control. Green tea catetechins have been found to increase leptin levels in the body. Leptin is a protein released from the hypothalamus that is involved in regulating body weight, initiating both food intake and energy expenditure. Increasing the level of leptin in the body is a mechanism that reduces appetite. (2)

BIOLOGICAL ACTIVITIES

Antiallergic activity

Catechin has been found to have a role in improving the symptoms of allergic disorders such as bronchial asthma and anaphylaxis in both human and animal studies. (6,7)

In studies revealing the anti-allergic properties of catechin and its pharmacological potential in this direction, it has been confirmed that antimicrobial, antiallergic and corticosteroid drugs that stabilize mast cells help stabilize mast cells. (8,9)

Concentration equal to or greater than 5 mM was able to stop the process of degranulate extrosis and reduced the number of mast cells degranulate.

While catechin was previously seen only as a source of antiallergic drugs to stabilize mast cells, it has been proven in the latest study that it inhibits exocytosis alone and shows antiallergic benefits by stabilizing mast cells. (6,7)

Based on all studies, while low concentrations of saciccatechin alone did not stabilize mast cells, they strengthened the mast cell stabilizing properties of antiallergic drugs and caffeine in synergy. At high concentrations, it showed an antiallergic effect by stabilizing mast cells alone. (8,9)

Antiangiogenesis activity

Angiogenesis plays an important role in the growth of tumors and lesions. Inhibition of angiogenesis is important to stop them. Catechins (EGCG) provide antiangiogenesis by acting on different cell mechanisms. Some of these mechanisms are as follows:

Mechanisms such as effect on the use of miRNAs, suppression of cell proliferation, induction of apoptosis, inhibition of the expression of angiogenic factors, suppression of phosphorylation of receptors, suppression

of VEGF receptor provide antiangiogenesis. Catechin, whose effect on such mechanisms has been discovered, comes to the fore in terms of antiangiogenesis properties. (10)

Antı-ınflammatory actıvıty

Inflammation is a kind of defense mechanism that protects organs from external factors and prevents infection. (11)

However, if the inflammatory response becomes chronic with overstimulation, it causes disease progression and adverse health effects. For this, it is important to control inflammation.(12)

Catechins have an anti-inflammatory effect and prevent inflammation during diseases.

It has been observed that inflammation during Alzheimer's disease and inflammation is suppressed by the passage of catechins decomposing in the small intestine into the brain tissue through the blood-brain barrier.(13)

Catechin repairs mitochondrial damage in the brain. Again, by stimulating different pathways in the brain, the catechin repaired the cognitive dysfunction and the inflammation that caused it. Catechins relieve inflammation during metabolic syndrome by reducing their inflammatory cytokines. (14)

Catechins can also play a role in relieving inflammation in the liver and respiratory tract. Catechin, which reduces the pressure on the liver with its effect on cholesterol, relaxes the respiratory tract by reducing pulmonary inflammation, and catechins establish the intestinal microbial balance by regulating the components of metabolites in the intestine. (15)

Catechins, which are not absorbed from the intestine and remain here, play an important role in relieving inflammation in the GIS. (16)

Antımıcrobıal actıvıty

The antimicrobial properties of catechins have long been studied.

As a result of these studies, it has been revealed that catechins fight organisms directly or indirectly. The anti-inflammatory effects of catechins also support these antimicrobial effects. Studies on E. Coli bacteria have shown that catechin has a significant effect on bacteria. (17,18)

Catechins have the ability to bind to the cell membrane of bacteria. This can have both a beneficial and sometimes harmful effect. (19,20,21)

Catechins are a flavonoid that can interfere with the activation of enzymes in the cell. Again, catechins can show a positive synergistic feature with some antibiotics in terms of their antibacterial properties. For this, it has been determined that their use together is beneficial. For example, it acts together with imipenem against MRSA. (21)

Antıfungal actıvıty

In studies with catechins, catechins have an effect on fungi such as Aspergillus, M. Canis, T. Mentagrophytes, T. Rubrum. Again, together with funcanazole, it has been revealed that they can work synergistically by inducing apoptosis on yeast fungi that are resistant to funcanazole. (22,23)

A*ntıvıral actıvıty*

Many studies have been conducted on the antiviral properties of catechins. Especially with studies with EGCG, the antiviral effect of catechins against DNA and RNA viruses has been observed. (24)

Table 5. Antiviral studies related to catechins

VIRUS	EFFECT	VIRUS	EFFECT
CILV	Inhibition of viral RNA replication (25)	HCV	Inhibition of viral entry into the target cell (34)
CILV	Inhibition of viral entry into target cells (26)	HIV	Reduction and suppression of Nf-kB expression (35)
CVB3	Inhibition of viral RNA replication (27)	HIV	Inhibition of viral replication (36)
EBV	It inhibits EBV by down-regulating RNA synthesis (28)	HIV	Suppressing viral infection ability, inhibiting viral(37)
HBV	Inhibition of HBsAg and HBeAg secretion) (29)	HIV	Inhibition of viral transcription (Calland et al.2012)(38)
HBV	Reducing HBV replication against HBV-	HSV	Activating viral (39)

	induced deficient autophagy (30)		
HBV	Inhibiting core promoter transcription (31)	ZIKA	Inhibition of viral entry into the target cell (40)
HBV	Inhibition of RNA, DNA, and cccDNA synthesis (32)	H1N1	Disruption of viral membrane integrity, prevention (41)
HCV	To interfere with and prevent virus adsorption (33)	H1N1	Inhibition of erythrocyte agglutination (42)

When experimenting with natural compounds with antiviral properties to be used as an adjunct to drugs used to bind and inhibit the SARS-COV-2 virus that causes the Covid 19 pandemic, the result seen is that Catechin binds and inhibits the virus more than other compounds. Thus, it has been recommended that those who are infected with this virus consume foods containing catechins excessively.

Effect on cholesterol

As a result of animal experiments on catechins, it has been determined that catechins reduce triglyceride and total cholesterol levels. Again, as a result of these experiments, it has been shown that it affects lipid metabolism by increasing energy use. (42,43)

Despite all these effects, the mechanism of action of catechin on cholesterol has not been resolved. As a result of a double-blind controlled study conducted for this purpose, it was observed that the cholesterol level of the group using catechins improved compared to the group not using catechins. Thus, one can talk about the good effect of catechin on cholesterol. (43)

Effect on copd

In studies on COPD, it has been observed that catechin increases the survival rate of human bronchial epithelial cells that are tried to be killed by cigarette smoke by looking at ROS formation. Again, in an extended study, it was observed that it inhibits inflammation in lung cells. (44)

Researchers thought that catechin has antioxidative and anti-inflammatory effects, and it was observed that Catechin reduced oxidative stress and inhibited the bad effects of the elements in the cells to which they gave various

foreign substances. Thus, they saw it as a potential treatment method against all respiratory diseases, especially COPD. (45)

Antımutagenıc actıvıty

Researchers who have been studying the mutation of cells for years have studied tea catechins to study the effects of catechins on mutagenicity.During these studies, it was primarily observed that Catechin blocks N-nitrosations very efficiently. That is, it revealed a rapid formation of bonds between nitrites and catechins. In another study, it was stated that catechin directly suppresses the mutation in activated fomes of Trp-P-2 and Glu-P-1 and reduces DNA single-strand breaks.Again, in the light of all these studies, it was seen that catechins had an effect on wing point test and DNA repairs, and as a result, reduced genotoxicity in such systems.

In order to benefit from the antimutagenic benefit of catechins, it is recommended to take them regularly and in sufficient concentration. (46, 47)

Cardıovascular Actıvıty

Catechins have special effects on the cardiovascular system. In the development of muscle strength, myofilament reduces Ca+2 sensitivity. It inhibits the myosin-actin interaction, causing muscle relaxation. (48) Catechins have the ability to regulate rhythmic actions in cardiac contraction by influencing the Ca+2 process in cardiomyocytes.

Catechins regulate the cycle of heart contraction by regulating SERCA2a, which is responsible for contraction in the heart. Considering all these effects, catechins are an effective form on cardiovascular system health. (49)

Antıobesıty Actıvıty

Obesity is seen by experts as the biggest and rapidly spreading disease of our time. One of the reasons for this is seen as triggering most diseases. The fact that catechins are a potential treatment method in terms of antiobesity has brought many experiments. In these studies, the effect of catechin on lipids and the inhibitions brought about by the apoptosis feature have been shown to have an antiobesity effect of catechin. (17)

Again, catechin is good for ROS and oxidative stress, which are considered as factors that increase obesity, and has a good effect on the development of obesityIn experiments, catechin consumption reduced body mass index, thinned waist and hip circumference, and decreased body and abdominal fat

in obese people. However, it has been concluded that it can help exercises in the weight loss process as it facilitates energy expenditure. (50)

Antıdıabetes Actıvıty

Diabetes is one of the most common diseases in the world. In addition, although diabetes is a disease, it is also a trigger of other diseases. Diabetes is not caused by a single mechanism, but by a network of mechanisms consisting of many signaling molecules. (51)

Catechins, on the other hand, can inhibit DM in a good way by affecting these multiple mechanisms. Catechins; improves insulin resistance, reduces oxidative stress, regulates mitochondrial function, reduces ER stress, has anti-inflammatory effects, reduces blood sugar sources, modulates intestinal functions. More studies are still needed for catechins, which are argued to be indirectly good for diabetes with these effects. (52)

Antıoxıdant Actıvıty

In vitro and in vivo studies have shown that catechin is a good antioxidant compound. (53) In studies conducted by Spizziri er al. in 2009, it showed the highest cytochiometry in reducing the rate of ABTS % during the administration of catechins. They also showed %ABTS cleaning activity. Again, at the oxidation rate called DHR123, it was seen that catechins defeated compounds with high oxidation. (54)

In cell modeling, catechins showed good protection against hemolysis caused by AAPH. Epicatechingallate has been discovered to be the most effective antioxidant against fluorescent bleaching caused by NaOCl. (55)

Oxidative stress is an imbalance of ROS and antioxidant systems. In the studies conducted by Lima et al. in 2009, it was determined that Catechin inhibits the ROS system and reduces oxidative stress on this functional disorder, which is the beginning of many diseases. (56)

In the light of all these studies, it would be the right choice to accept catechin as a high-functioning antioxidant compound and use it in this direction. Still, many studies are needed to grasp the true antioxidant potential of catechin. (57)

Neuroprotective Activity

Neurodegeneration is the loss of structure and function in neurons, including the death of neurons. Many diseases, especially Alzheimer's and Parkinson's, occur due to neurodegeneration. (58)

Factors affecting neurodegeneration; environmental factors, mitochondrial dysfunction, age and family history, ROS, synaptic injuries, metal uptake, protein disorders. (59)

In recent years, experts have taken action for neurodegeneration, which is the beginning of the most common disorders due to the increasing elderly population, and have focused on the treatment of neurodegenerative diseases. (60)

In studies with catechins, it has been observed that catechin is beneficial against neurodegenerative diseases as a potential neuroprotective. (61)

Table 6. Neuroprotective studies of catechin

Experımental Model	Dısease	Result
Laboratory	Alzheimer's	Inhibition of tau aggregation and oxidation (George et al.2013) (62)
Laboratory	Huntington's disease	Inhibitory effect on htt aggregation (63)
Mouse	Parkinson's disease	It improves rotational behavior, mobility, and memory. (64)
Mouse	Alzheimer's	It reduces oxidative stress and shows cholinergic improvement. improvement in synaptic and mitochondrial functions. (65)

Mouse	Multiple sclerosis	Reduces the onset and clinical severity of the disease. Reduces inflammatory leaks. (66)
Drosophila	Huntington's disease	can modulate symptoms. (67)
Human being	Multiple sclerosis	Improves muscle metabolism, prevents NOX and overactivation, reduces plasma NAA levels. (68)
Human being	Down syndrome	Improves visual recognition memory. (69)
Human being	Alzheimer's	The low prevalence of cognitive impairment is associated with a decrease in oxidative stress and reduces lipid peroxidation. (70)

Antıcancer Actıvıty

Cancers (malignant tumors, malignant tumors) are usually continuous and fast-growing tumors. They do not have capsules, they know no boundaries when growing, they penetrate into the surrounding tissues and vessels (invasion, infiltrative growth). They often metastasize. Untreated or delayed cancers are fatal.

In modern medicine, it is predicted that in order for a formation to be called "cancer", it must contain 5 qualities; (71,72)

Unlimited proliferation ability in cells. Insensitivity to factors that inhibit its growth. Immortality of its cells (absence of apoptosis). Ability to stimulate the formation of new vessels (angiogenesis). Factors such as its ability to enter tissues (invasion) and form new colonies (metastasis) are the characteristics of catechin. Experts have discussed catechin as a potential treatment method that has turned out to be an obstacle to these qualities. As a result of the experiments, striking results were obtained. The anticancer effect of catechin has been shown by many studies to act in more than one type of cancer.

When catechins are taken in the lungs and orally, they prevent the formation of cancer in the prostate. Abnormal DNA methylation and tumor formation are a factor in the onset and progression of cancer. The antitumor effect of catechin reveals its anticancer effect. (36)

As a result of in vivo studies, catechins have been found to suppress colon cancer cells by inhibiting VEGF, and this is due to the angiogenic effect of catechins. (73)

It would not be wrong to talk about a similar situation in studies conducted in human pancreas and breast cells. In suppressing cancer in human colorectal cells, it has been observed that catechins suppress EGFR and PDGFR.Catechin is one of the natural components that received a passing grade in terms of preventing tumor migration, which is one of the most common effects in ensuring the spread of cancer. This is considered to be one of the anticancer effects of catechin. (74) One of the anticancer effects of catechin is considered to be inducing apoptosis.Apoptosis; Catechin acts separately on 5 different forms: caspase-dependent, caspase-independent, mediated by lysosomal membrane permeability, autophagy and adjuvant. Various studies have shown that catechin helps in the inhibition of the Bcl-2 protein family in a caspase-dependent manner and induces apoptosis by down-

regulation in nasopharyngeal casino, prostate carcinoma, breast carcinoma, hepatoma cell carcinoma, bladder and ovarian carcinoma cells. Catechins cause apoptosis in laryngeal epidermoid carcinoma cells independently of caspase. (75) Autophagy refers to cell death through the breakdown of cellular components. Although there are results that catechin supports autophage, further studies are needed. (76)

The use of catechins as adjuvants may increase anticancer activity. In order to break the multi-drug resistance in tumors, catechins work in harmony with drugs. It has been observed that catechins benefit the patient when given together with the drug in multidrug-resistant breast carcinoma and kidney carcinoma cells. (77) Catechins have an anticancer effect by modulating signaling molecules. Catechins, which clean ROS, indirectly inhibit cancer formation with their antioxidant properties. Catechins, which have a strengthening effect on extracellular signals (such as chemotherapy) called nuclear factor-B and MAPK, have an indirect anticancer effect. As a result of all these ongoing studies, catechins stand out as a potential anticancer treatment component directly or indirectly, depending on the concentration. (78)

Table 7. Anticancer activity studies with catechins

Workıng Model	Bıologıcal Effect
Leukemia T cells	Cell cycle and growth arresting effect. (79)
Human colon carcinoma cells	It provides inhibition of nitric oxide inside the cell. (80)
Mouse macrophages	Inhibition of cell proliferation and apoptosis effect. (80)
Human leukemia Raji B cells	Induction of apoptosis. (81)
Human breast cancer cells	Inhibition of cell growth and cell proliferation. (82)

Human lymphoma cells	Formation of apoptosis, ROS formation. (83)
Human colon cancer cells	It is a potent inhibitor of DNA polymerase activity. (84)

RESULT

Studies on catechin have been associated with a variety of direct and indirect activities. However, although they have a high potential for some activities, more experimental studies are needed before full activation can be proven. The great advantage of the catechin is that it is a natural ingredient, in addition to embodying many different activities. Therefore, catechin, which can exert beneficial biological effects on the body when taken in the right doses, should be taken with catechin-rich foods. The potential of catechins and their natural origin offer an important option for health. However, more research is needed before its full effects can be understood. The results of these studies will help us better understand the effects of catechins on health and ensure optimal benefit.

REFERENCE

1.Farhan, M. (2022). Greenteacatechins: nature'sway of preventingandtreatingcancer. International journal of molecularsciences, 23(18), 10713.

2. NURTEN, D. D. A., & ZENGİN, A. SIÇAN FRENİK SİNİR-HEMİDİYAFRAM PREPARATINA ANTİOKSİDAN RESVERATROL, KATEŞİN VE EPİKATEŞİNİN ETKİLERİ.2007

3.Musial, C., Kuban-Jankowska, A., &Gorska-Ponikowska, M. (2020). Beneficialproperties of greenteacatechins. International journal of molecularsciences, 21(5), 1744.

4.Üstün, Ç., & Demirci, N. (2013). Çay bitkisinin (camelliasınensıs l.) tarihsel gelişimi ve tıbbi açıdan değerlendirilmesi. Mersin Üniversitesi Tıp Fakültesi Lokman Hekim Tıp Tarihi ve Folklorik Tıp Dergisi, 3(3), 5-12.

5.Fidan, I., &Cenik, Y. (1976). Şaraplarda Kateşin Miktarı Üzerinde Araştırmalar. Gıda, 1(2).

6.Shin HY, Lee CS, Chae HJ, Kim HR, Baek SH, An NH, et al. Inhibitoryeffectofanaphylacticshockbycaffeine in rats. Int J Immunopharmacol. 2000;22:411–

7.Bani D, Giannini L, Ciampa A, Masini E, Suzuki Y, Menegazzi M, et al.Epigallocatechin-3-gallate reducesallergen-inducedasthma-likereaction in sensitizedguineapigs. J PharmacolExpTher. 2006;317:1002–11.

8.Baba A, Tachi M, Maruyama Y, Kazama I. Olopatadineinhibitsexocytosis in ratperitonealmastcellsbycounteractingmembranesurfacedeformation. Cell Physiol Biochem.2015;35:386–96.

9.Abe N, Toyama H, Ejima Y, Saito K, Tamada T, Yamauchi M, et al. Alpha 1-adrenergic receptorblockadebyprazosinsynergisticallystabilizesratperitonealmastcells. BiomedResInt. 2020;2020:3214186.

10.Rashidi, B., Malekzadeh, M., Goodarzi, M., Masoudifar, A., & Mirzaei, H. (2017). Green tea and its anti-angiogenesis effects. Biomedicine & Pharmacotherapy, 89, 949-956.

11.Lomax AR andCalder PC. Probiotics, immunefunction, infectionandinflammation: a review of theevidencefromstudiesconducted in humans. CurrentPharmaceutical Design. 15:1428-1518 (2009)

12.Ferrucci, L, Fabbri E. Inflammageing: chronicinflammation in ageing, cardiovasculardisease, andfrailty. Nature ReviewsCardiology. 15: 505-522 (2018)

13.Unno K, Pervin M, Nakagawa A, Iguchi K, Hara A, Takagaki A, Nanjo F, Minami A, Nakamura Y. Blood–brainbarrier perme- ability of greenteacatechinmetabolitesandtheirneuritogenicactivity in humanneuroblastoma SH-SY5Y cells. MolecularNutrition&FoodResearch. 61: 1700294 (2017)

14.Kim JM, Lee U, Kang JY, Park SK, Kim JC, Heo HJ. Matchaimprovesmetabolicimbalance-inducedcognitivedysfunction. OxidativeMedicineand Cellular Longevity. 2020: 8882763(2020b)

15.Forester SC, Gu Y, Lambert JD. Inhibition of starchdigestionbythegreenteapolyphenol, (-)-epigallocatechin-3-gallate. MolecularNutrition&FoodResearch. 56: 1647-1654 (2012)

16.Kim JM, Park SK, Kang JY, Park SB, Yoo SK, Han HJ, Kim CW,Lee U, Kim SH, Heo HJ. Ethylacetatefractionfrompersimmon (Diospyroskaki) amelioratescerebralneuronallossandcogni- tivedeficitviathe JNK/Aktpathway in TMT-inducedmice. International Journal of MolecularSciences. 19: 1499 (2018)

17.Moon HS, Chung CS, Lee HG, Kim TG, Choi YJ, Cho CS. Inhibitoryeffect of (−)-epigallocatechin-3-gallate on lipid accumulation of 3T3-L1 cells. Obesity. 2007; 15:2571–2582.[PubMed: 18070748]

18.T. W. Sirk, E. F. Brown, A. K. Sum, and M. Friedman, "Moleculardynamicsstudy on thebiophysicalinteractions of seven greenteacatechinswith lipid bilayers of

cellmembranes," Journal of AgriculturalandFoodChemistry, vol. 56, no. 17, pp. 7750–7758,2008.

19.J. Steinmann, J. Buer, T. Pietschmann, and E. Steinmann, "Anti-infectiveproperties of epigallocatechin-3-gallate (EGCG), acomponent of greentea," British Journal of Pharmacology, vol.168, no. 5, pp. 1059–1073, 2013.

20.O. Levinger, T. Bikels-Goshen, E. Landau, M. Fichman, and R. Shapira, "Epigallocatechingallateinducesupregulation of the two-componentVraSRsystembyevoking a cellwallstressresponse in Staphylococcusaureus," AppliedandEnvironmentalMicrobiology, vol. 78, no. 22, pp. 7954–7959, 2012.

21.P. D. Stapleton, S. Shah, K. Ehlert, Y. Hara, and P. W. Taylor,"Theβ-lactam-resistancemodifier (-)-epicatechingallatealtersthearchitecture of thecellwall of Staphylococcusaureas,"Microbiology, vol. 153, no. 7, pp. 2093–2103, 2007.

22.C. R. Da Silva, J. B. De AndradeNeto, R. De SousaCampos et al., "Synergisticeffect of the flavonoid catechin, quercetin, orepigallocatechingallatewithfluconazoleinduces apoptosis in Candidatropicalisresistanttofluconazole," AntimicrobialAgentsandChemotherapy, vol. 58, no. 3, pp. 1468–1478, 2014

23.A. Thomas, S. Thakur, R. Habib, and N. Marwah, "Comparison of AntimicrobialEfficacy of GreenTea, Garlicwith Lime, andSodiumFluorideMouthRinsesagainstStreptococcusmutans, Lactobacillispecies, andCandidaalbicans in Children: A Ran- domizedDouble-blindControlledClinical Trial," International Journal of ClinicalPediatricDentistry, vol. 10, no. 3, pp. 234–239,2017.

24. Zhong, L.; Hu, J.; Shu, W.; Gao, B.; Xiong, S. Epigallocatechin-3-gallate opposes HBV-inducedincompleteautophagybyenhancinglysosomalacidification, which is unfavorablefor HBV replication. Cell DeathDis. 2015, 6. [CrossRef] [PubMed]

24.Ho, H.Y.; Cheng, M.L.; Weng, S.F.; Leu, Y.L.; Chiu, D.T.Y. Antiviral effect of Epigallocatechingallate on Enterovirus 71. J. Agric.FoodChem. 2009, 57, 6140–6147. [CrossRef] [PubMed]

26.Carneiro, B.M.; Batista, M.N.; Braga, A.C.S.; Nogueira, M.L.; Rahal, P. Thegreenteamolecule EGCG inhibitsZikavirusentry.Virology 2016, 496, 215–218. [CrossRef] [PubMed]

27. Weber, C.; Silva, K.; vonRhein, C.; Kuemmerer, B.M.; Schnierle, B.S. Thegreenteacatechin, epigallocatechingallateinhibitsChikungunyavirusinfection. Antivir. Res. 2015, 113, 1–3. [CrossRef] [PubMed]

28. Lu, J.W.; Hsieh, P.S.; Lin, C.C.; Hu, M.K.; Huang, S.M.; Wang, Y.M.; Liang, C.Y.; Gong, Z.Y.; Ho, Y.J. Synergisticeffectsofcombinationtreatmentusing EGCG andSuraminagainsttheChikungunyavirus. Biochem. Biophys. Res. Commun. 2017, 491,595–602. [CrossRef]

29.Fassina, G.; Buffa, A.; Benelli, R.; Varnier, O.E.; Noonan, D.M.; Albini, A. Polyphenolicantioxidant (−)-Epigallocatechin-3-gallate fromgreentea as a candidate anti-HIV agent. Aids 2002, 16, 939–941. [CrossRef] [PubMed]

30.Kumar, D.; Sharma, N.; Aarthy, M.; Singh, S.K.; Giri, R. MechanisticinsightsintoZikavirus NS3 helicaseinhibitionby Epigallocatechin-3-gallate. ACS Omega 2020, 5, 11217–11226. [CrossRef]

31.Xu, J.; Gu, W.; Li, C.; Li, X.; Xing, G.; Li, Y.; Song, Y.; Zheng, W. Epigallocatechingallateinhibitshepatitis B virusviafarnesoid X receptoralpha. J. Nat. Med. 2016, 70, 584–591. [CrossRef] [PubMed]

32.Zhong, L.; Hu, J.; Shu, W.; Gao, B.; Xiong, S. Epigallocatechin-3-gallate opposes HBV-inducedincompleteautophagybyenhancinglysosomalacidification, which is unfavorablefor HBV replication. Cell DeathDis. 2015, 6. [CrossRef] [PubMed]

33.Pang, J.Y.; Zhao, K.J.; Wang, J.B.; Ma, Z.J.; Xiao, X.H. Greenteapolyphenol, Epigallocatechin-3-gallate, possessesthe antiviralactivitynecessarytofightagainstthehepatitis B virusreplication in vitro. J. ZhejiangUniv. Sci. B 2014, 15, 533–539.[CrossRef] [PubMed]

34.He, W.; Li, L.X.; Liao, Q.J.; Liu, C.L.; Chen, X.L. Epigallocatechingallateinhibits HBV DNA synthesis in a viral replication-induciblecellline. World J. Gastroenterol. 2011, 17, 1507–1514. [CrossRef]

35.Isaacs, C.E.; Wen, G.Y.; Xu, W.; Jia, J.H.; Rohan, L.; Corbo, C.; DiMaggio, V.; Jenkins, E.C., Jr.; Hillier, S. Epigallocatechingallateinactivatesclinicalisolates of herpessimplexvirus. Antimicrob. AgentsChemother. 2008, 52, 962–970. [CrossRef]

36.Liu, S.; Li, H.; Chen, L.; Yang, L.; Li, L.; Tao, Y.; Li, W.; Li, Z.; Liu, H.; Tang, M.; et al. (−)-Epigallocatechin-3-gallate inhibition of Epstein-Barrvirusspontaneouslyticinfectioninvolves ERK1/2 and PI3-K/Aktsignaling in EBV-positivecells. Carcinogenesis 2013, 34, 627–637. [CrossRef]

37.An Y, Li Z, Wang S, Wang Z. Inhibition of (–)epigallocatechin gallate on dimethylarsinic acid promoting lung tumorigenesis through the induction of oxidative stress in mice. Wei Sheng Yan Jiu 2008;37:748–50

38.Calland, N.; Albecka, A.; Belouzard, S.; Wychowski, C.; Duverlie, G.; Descamps, V.; Hober, D.; Dubuisson, J.; Rouille, Y.; Seron, K.(−)-Epigallocatechin-3-gallate is a newinhibitor of hepatitis C virusentry. Hepatology 2012, 55, 720–729. [CrossRef]

39.Ciesek, S.; vonHahn, T.; Colpitts, C.C.; Schang, L.M.; Friesland, M.; Steinmann, J.; Manns, M.P.; Ott, M.; Wedemeyer, H.;Meuleman, P.; et al. Thegreenteapolyphenol, epigallocatechin-3-gallate, inhibitshepatitis C virusentry. Hepatology 2011, 54, 1947–1955. [CrossRef]

40.Kim, M.; Kim, S.Y.; Lee, H.W.; Shin, J.S.; Kim, P.; Jung, Y.S.; Jeong, H.S.; Hyun, J.K.; Lee, C.K. Inhibition of influenza virüs internalizationby (−)-Epigallocatechin-3-gallate. Antivir. Res. 2013, 100, 460–472. [CrossRef]

41.Song, J.M.; Lee, K.H.; Seong, B.L. Antiviral effect of catechins in greentea on influenza virus. Antivir. Res. 2005, 68,66–74. [CrossRef]

42.Li, S.; Hattori, T.; Kodama, E.N. Epigallocatechingallateinhibitsthe HIV reversetranscription step. Antivir. Chem. Chemother.2011, 21, 239–243. [CrossRef]

42.Koo SI andNoh SK: Greentea as inhibitor of the intestinal absorption of lipids: potentialmechanismforits lipid-loweringeffect. J NutrBiochem 18: 179-183, 2007.

43.Murase T, Haramizu S, Shimotoyodome A, Tokimitsu I andHase T: Greenteaextractimprovesrunningendurance in micebystimulating lipid utilizationduringexercise. Am J PhysiolRegulIntegrCompPhysiol 290: R1550-R1556, 2006.

44.M. Rudrapal, S. Maji, S.K. Prajapati, P. Kesharwani,P.K. Deb, J. Khan, ...and A.R. Bendale, "Protectiveeffects of dietsrich in polyphenols in cigarettesmoke (CS)-inducedoxidativedamagesandassociatedhealthimplications". Antioxidants, vol.11, pp.1217, 2022.

45.S.P. Lakshmi, A.T. Reddy, L.D. Kodidhela, N.C.Varadacharyulu, "EpigallocatechinGallateDiminishesCigaretteSmoke-InducedOxidativeStress, Lipid Peroxidation, andInflammation in Human BronchialEpithelialCells". Life Sci. vol.259, 118260, 2020

46.J.H. Weisburger, M. Nagao, K. Wakabayashi, A. Oguri,Prevention of heterocyclic amine formationbyteaandteapolyphenols, CancerLett. 83 (1994) 143–147

47.H. Hayatsu, N. Inada, T. Kakutani, S. Arimoto, T. Negishi,K. Mori, T. Okuda, I. Sakata, Suppression of genotoxicity of carcinogensby (−)-epigallocatechingallate, Prev. Med.21 (1992) 370–376.

48.Spyracopoulos, L.; Li, M.X.; Sia, S.K.; Gagné, S.M.; Chandra, M.;Solaro, R.J.; Sykes, B.D. Calcium-inducedstructuraltransition in theregulatory domain of humancardiactroponin C. Biochemistry,1997, 36(40), 12138-12146. http://dx.doi.org/10.1021/bi971223d PMID: 9315850

49.Thakur, V.S.; Gupta, K.; Gupta, S. Greenteapolyphenolsincrease p53 transcriptionalactivityandacetylationbysuppressingclass I histonedeacetylases. Int. J. Oncol., 2012, 41(1), 353-361.PMID: 22552582

50. Alvehus M, Buren J, Sjostrom M, Goedecke J, Olsson T. Thehumanvisceralfatdepot has a uniqueinflammatory profile. Obesity. 2010; 18:879–883. [PubMed: 20186138]

51.Bommer, C.; Sagalova, V.; Heesemann, E.; Manne-Goehler, J.; Atun, R.; Bärnighausen, T.; Davies, J.; Vollmer, S. Global EconomicBurden of Diabetes in Adults: ProjectionsFrom 2015 to 2030. DiabetesCare 2018, 41, 963–970. [CrossRef] [PubMed]

52.Diagnosis andclassification of diabetesmellitus. DiabetesCare 2013, 36 (Suppl. 1), S67–S74. [CrossRef] [PubMed]

53 Bae, J., Kim, N., Shin, Y., Kim, S. Y., & Kim, Y. J. (2020). Activity of catechins and their applications. Biomedical Dermatology, 4, 1-10..

54.Spizzirri UG, Iemma F, Puoci F, Cirillo G, Curcio M, Parisi OI, et al. Synthesis of antioxidant polymers by grafting of gallic acid and catechin on gelatin. Biomacromolecules. 2009;10:1923 –30.

55.Feng B, Fang Y, Wei SM. Effect and mechanism of epigallocatechin-3-gallate (EGCG) against the hydrogen peroxide-induced oxidative damage in human dermal fibroblasts. J Cosmet Sci. 2013;64(1):35–44.

56.Lima EBC, de Sousa CNS, Vasconcelos GS, Meneses LN, YF e SP, Ximenes NC, et al. Antidepressant, antioxidant and neurotrophic properties of the standardized extract of Cocos nucifera husk fiber in mice. J Nat Med. 2016;70: 510–21

57.Zhang W, Yang Y, Lv T, Fan Z, Xu Y, Yin J, et al. Sucrose esters improve the colloidal stability of nanoethosomal suspensions of (−)-epigallocatechin gallate for enhancing the effectiveness against UVB-induced skin damage. J Biomed Mater Res B Appl Biomater. 2016;105:2416 –25.

58.Mähler, A.; Steiniger, J.; Bock, M.; Klug, L.; Parreidt, N.; Lorenz, M.; Zimmermann, B.F.; Krannich, A.; Paul, F.; Boschmann, M. Metabolicresponseto epigallocatechin-3-gallate in relapsing-remitting multiple sclerosis: A randomizedclinicaltrial. Am. J. Clin. Nutr. 2015, 101, 487–495. [CrossRef] [PubMed]

59.Lovera, J.; Ramos, A.; Devier, D.; Garrison, V.; Kovner, B.; Reza, T.; Koop, D.; Rooney, W.; Foundas, A.; Bourdette, D. PolyphenonE, non-futile at neuroprotection in multiple sclerosis but unpredictablyhepatotoxic: Phase I singlegroupandphase II randomizedplacebo-controlledstudies. J. Neurol. Sci. 2015, 358, 46–52. [CrossRef]

60.Ide, K.; Yamada, H.; Takuma, N.; Kawasaki, Y.; Harada, S.; Nakase, J.; Ukawa, Y.; Sagesaka, Y.M. Effects of greenteaconsumptionon cognitivedysfunction in an elderlypopulation: A randomizedplacebo-controlledstudy. Nutr. J. 2016, 15, 49. [CrossRef]

61.de la Torre, R.; de Sola, S.; Hernandez, G.; Farré, M.; Pujol, J.; Rodriguez, J.; Espadaler, J.M.; Langohr, K.; Cuenca-Royo, A.; Principe, A.; et al. Safetyandefficacy of cognitivetrainingplus epigallocatechin-3-gallate in youngadultswithDown'ssyndrome(TESDAD): A double-blind, randomised, placebo-controlled, phase 2 trial. Lancet Neurol. 2016, 15, 801–810. [CrossRef]

62.George, R.C.; Lew, J.; Graves, D.J. Interaction of cinnamaldehydeandepicatechinwithtau: Implications of beneficialeffects in modulatingAlzheimer'sdiseasepathogenesis. J. Alzheimer'sDis. JAD 2013, 36, 21–40. [CrossRef]

63.Beasley, M.; Stonebraker, A.R.; Hasan, I.; Kapp, K.L.; Liang, B.J.; Agarwal, G.; Groover, S.; Sedighi, F.; Legleiter, J. Lipid MembranesInfluencetheAbility of Small MoleculesToInhibitHuntingtinFibrillization. Biochemistry 2019, 58, 4361– [CrossRef]

64.Teixeira, M.D.; Souza, C.M.; Menezes, A.P.; Carmo, M.R.; Fonteles, A.A.; Gurgel, J.P.; Lima, F.A.; Viana, G.S.; Andrade, G.M. Catechinattenuatesbehavioralneurotoxicityinducedby 6-OHDA in rats. Pharmacol. Behav. 2013, 110, 1–7. [CrossRef]

65.Al-Amri, J.S.; Hagras, M.M.; Mohamed, I.M. Effect of epigallocatechin-3-gallate on inflammatorymediatorsrelease in LPS-inducedParkinson'sdisease in rats. Indian J. Exp. Biol. 2013, 51, 357–362.

66.Jelenkoviˊc, A.; Jovanoviˊc, M.D.; Stevanoviˊc, I.; Petronijeviˊc, N.; Bokonjiˊc, D.; Zivkoviˊc, J.; Igiˊc, R. Influence of thegreentealeafextract on neurotoxicity of aluminiumchloride in rats. Phytother. Res. PTR 2014, 28, 82–87. [CrossRef]

67.Herges, K.; Millward, J.M.; Hentschel, N.; Infante-Duarte, C.; Aktas, O.; Zipp, F. Neuroprotectiveeffect of combinationtherapy of glatirameracetateand epigallocatechin-3-gallate in neuroinflammation. PLoS ONE 2011, 6, e25456. [CrossRef] [PubMed]

68.Semnani, M.; Mashayekhi, F.; Azarnia, M.; Salehi, Z. Effects of greentea epigallocatechin-3-gallate on theproteolipid protein andoligodendrocytetranscriptionfactor 1 messenger RNA gene expression in a mouse model of multiple sclerosis. Folia Neuropathol.2017, 55, 199–205. [CrossRef] [PubMed]

69.Varga, J.; Dér, N.P.; Zsindely, N.; Bodai, L. Greenteainfusionalleviatesneurodegenerationinducedby mutant Huntingtin in Drosophila. Nutr. Neurosci. 2020, 23, 183–189. [CrossRef] [PubMed]

70.Kuriyama, S.; Hozawa, A.; Ohmori, K.; Shimazu, T.; Matsui, T.; Ebihara, S.; Awata, S.; Nagatomi, R.; Arai, H.; Tsuji, I. Greenteaconsumptionandcognitivefunction: A cross-sectionalstudyfromtheTsurugaya Project. Am. J. Clin. Nutr. 2006, 83, 355–361.

71.Katiyar S, Mukhtar H. Tea in chemoprevention of cancer. Int J Oncol 1996;8:221–38.

72.Schramm L. Going green: the role of the green tea component EGCG in chemoprevention. J Carcinog Mutagen 2013;4:1000142–56.

73.Shankar S, Marsh L, Srivastava RK. EGCG inhibits growth of human pancreatic tumors orthotopically implanted in Balb C nude mice through modulation of FKHRL1/FOXO3a and neuropilin. Mol Cell Biochem 2013;372:83–94.

74.Zhang Y, Han G, Fan B, Zhou Y, Zhou X, Wei L, et al. Green tea (–)-epigallocatechin-3-gallate down-regulates VASP expression and inhibits breast cancer cell migration and invasion by attenuating Rac1 activity. Eur J Pharmacol 2009;606:172–9

75.Lee JH, Jeong YJ, Lee SW, Kim D, Oh SJ, Lim HS, et al. EGCG induces apoptosis in human laryngeal epidermoid carcinoma Hep2 cells via mitochondria with the release of apoptosis-inducing factor and endonuclease G. Cancer Lett 2010;290:68–75

75.Zhao Y, Yang LF, Ye M, Gu HH, Cao Y. Induction of apoptosis by epigallocatechin-3-gallate via mitochondrial signal transduction pathway. Prev Med 2004;39:1172–9.

76.Li CP, Yao J, Tao ZF, Li XM, Jiang Q, Yan B. Epigallocatechin-gallate (EGCG) regulates autophagy in human retinal pigment epithelial cells: a potential role for reducing UVB light-induced retinal damage. Biochem Biophys Res Commun 2013;438:739–45.

77.Farabegoli F, Papi A, Bartolini G, Ostan R, Orlandi M. (–)-Epigallocatechin-3-gallate downregulates Pg-P and BCRP in a tamoxifen resistant MCF-7 cell line. Phytomedicine 2010;17:356–62

78.Ge J, Tan BX, Chen Y, Yang L, Peng XC, Li HZ, et al. Interaction of green tea polyphenol epigallocatechin-3-gallate with sunitinib: potential risk of diminished sunitinib bioavailability. J Mol Med (Berl) 2011;89:595–602.

79.Lam, W. H., Kazi, A., Kuhn, D. J., Chow, L. M. C., Chan, A. S. C., Ping Dou, Q., & Chan, T. H. (2004). A potential prodrug for a green tea polyphenol proteasome inhibitor: Evaluation of the peracetate ester of (-)-epigallocatechin gallate [(-)-EGCG]. Bioorganic and Medicinal Chemistry, 12(21), 5587–5593.

80.Lambert, J. D., Sang, S., Hong, J., Kwon, S. J., Lee, M. J., Ho, C. T., & Yang, C. S. (2006). Peracetylation as a means of enhancing in vitro bioactivity and bioavailability of epigallocatechin-3-gallate. Drug Metabolism and Disposition, 34(12), 2111–2116

81.Sierra, H., Cordova, M., Chen, C. S. J., & Rajadhyaksha, M. (2015). Confocal imagingguided laser ablation of basal cell carcinomas: An ex vivo study. Journal of Investigative Dermatology, 135(2), 612–615.

82.Wang, C. C., Xu, H., Man, G. C. W., Zhang, T., Chu, K. O., Chu, C. Y., ... Chan, T. H. (2013). Prodrug of green tea epigallocatechin-3-gallate (Pro-EGCG) as a potent anti-angiogenesis agent for endometriosis.

83.Ahmed, K., Wei, Z., Zhao, Q., Nakajima, N., Matsunaga, T., Ogasawara, M., & Kondo, T. (2010). Chemico-Biological Interactions Role of fatty acid chain length on the induction of apoptosis by newly synthesized catechin derivatives. Chemico-Biological Interactions, 185(3), 182–188.

84.Mizushina, Y., Saito, A., Horikawa, K., Nakajima, N., Tanaka, K., Yoshida, H., & Matsubara, K. (2011). Acylated catechin derivatives: Inhibitors of DNA polymerase and angiogenesis. Frontiers in Biosience, 3, 1337–1348.

Dynamics and Hopf Bifurcation in an SIRS Model with Logistic Growth and Saturated Treatment Effects

İrem ÇAY[1]

1- Res. Asst. Dr.; Kocaeli Üniversitesi Fen - Edebiyat Fakültesi Matematik Bölümü. irem.atac@kocaeli.edu.tr ORCID No: 0000 – 0001 – 9234 – 2523

ABSTRACT

In the current work, we investigate an epidemic model that incorporates both saturated treatment and logistic population growth. We derive sufficient conditions under which bifurcations may occur within the system. Furthermore, to validate the analytical findings, we present several numerical simulations that illustrate the dynamical behavior of the model under varying parameter regimes.

Keywords – Epidemic model, Stability, Bifurcation, Logistic growth, Saturated Treatment.

INTRODUCTION

The mathematical modeling of infectious diseases has become an indispensable tool for understanding the transmission dynamics of epidemics and for designing effective control strategies. Among the classical compartmental models, the Susceptible–Infectious–Recovered–Susceptible (SIRS) framework is particularly relevant for diseases that do not confer permanent immunity, allowing individuals to return to the susceptible class after a period of recovery. Such models are especially applicable to recurrent infectious diseases such as influenza, pertussis, and COVID-19.

Several recent studies have extended the classical SIRS framework to account for factors such as partial immunity, co-infection dynamics, and waning immunity, especially in the context of diseases like COVID-19 and influenza (El Khalifi & Britton, 2022; Zafarnejad, Griffin, & Ventresca, 2022; Bhowmick, Sokolov, & Lentz, 2022; Nesteruk, 2024; Imran, McKinney, & Butt, 2025).

In real-world scenarios, epidemic dynamics are often influenced by a combination of demographic and treatment-related factors. Logistic population growth accounts for the limited environmental carrying capacity and provides a more realistic representation of population dynamics compared to models with constant population size. Additionally, the assumption of unlimited treatment resources is rarely practical, especially in the context of large-scale outbreaks. To address this, saturated treatment functions have been introduced to capture the diminishing effectiveness of treatment as the number of infected individuals increases, reflecting the constraints of healthcare infrastructure.

In this study, we investigate the stability and dynamic behavior of an SIRS epidemic model incorporating logistic growth and a saturated treatment response. We conduct a comprehensive analysis of the equilibrium points and determine the conditions under which the disease-free and endemic equilibria are locally asymptotically stable. Furthermore, we explore the possibility of Hopf bifurcation arising from changes in model parameters, which may lead to the emergence of sustained oscillations in the number of infected individuals. Understanding these bifurcations is crucial for predicting periodic outbreaks and for informing timely public health interventions.

By integrating logistic growth and treatment saturation into the classical SIRS model, this work aims to provide deeper insights into the complex interplay between population dynamics, resource limitations, and disease transmission. The analytical findings are complemented by numerical simulations to illustrate the rich dynamical behaviors exhibited by the model under various parameter regimes.

To gain a deeper understanding of the system's dynamics, we construct a deterministic compartmental model governed by a system of nonlinear ordinary differential equations. The total population is partitioned into three distinct epidemiological classes: susceptible individuals $S(t)$, infected individuals $I(t)$, and recovered individuals $R(t)$. The model incorporates logistic population growth to reflect natural birth and death processes under limited environmental capacity, and a saturated treatment response to account for limitations in medical resources during outbreaks. The treatment saturation is modeled through a nonlinear function that captures the diminishing per capita treatment rate as the number of infections increases.

The proposed model extends the classical SIRS framework by integrating these realistic features and aims to capture the complex interplay between population dynamics, disease transmission, recovery, and healthcare limitations. In the next section, we present the mathematical formulation of the model, provide a detailed description of all parameters and state variables, and establish the fundamental properties of the model. These foundational results set the stage for the subsequent analysis of equilibrium points, local stability, and the conditions leading to Hopf bifurcation.

Mathematical Model

In this section, we develop an SIRS epidemic model that accounts for logistic population growth and includes a saturated treatment response. The total population at time t, represented by $N(t) = S(t) + I(t) + R(t)$, is categorized into three distinct compartments: susceptible individuals $S(t)$, infected individuals $I(t)$, and recovered individuals $R(t)$. The evolution of these compartments over time is described as follows:

$$\frac{dS(t)}{dt} = \alpha\, S(t)\left(1 - \frac{S(t)}{K}\right) - \beta\, S(t)I(t) + \delta\, R(t), \tag{1}$$

$$\frac{dI(t)}{dt} = \beta\, S(t)I(t) - (\rho + \gamma)I(t) - \frac{rI(t)}{1 + \epsilon\, I(t)}, \tag{2}$$

$$\frac{dR(t)}{dt} = \gamma\, I(t) - (\rho + \delta)R(t) + \frac{rI(t)}{1 + \epsilon\, I(t)}. \tag{3}$$

where each term is given the following table.

Table 1: Definition of parameters

Parameters	Definition
α	intrinsic growth rate of the susceptible population
K	environmental carrying capacity
β	transmission rate of the infection
δ	the immunity loss rate transitioning recovered individuals back to the susceptible compartment.
ρ	natural death rate
γ	natural recovery rate of infected individuals,
r	maximum treatment rate
ϵ	saturation parameter of the treatment function

Equilibria and Local Dynamics

In this section, we conduct a local stability analysis of the model system (1)–(3). A critical threshold parameter, the basic reproduction number R_0, plays a central role in determining the stability of the system's equilibrium points. This value reflects the average transmission potential of an infected individual within a population where all individuals are susceptible. We derive the expression for the basic reproduction number R_0 corresponding to the model equations (1)–(3) as follows.

$$R_0 = \frac{K\,\beta}{\rho + \gamma + r}. \tag{4}$$

The model (1)-(3) has following equilibria:

- the disease-free equilibrium $E^0 = (K, 0, 0,)$,
- the endemic equilibrium $E^* = (S^*, I^*, R^*)$. Here

$S^* = \frac{1}{\beta}\left(\rho + \gamma + \frac{r}{1+\epsilon I^*}\right)$,

$R^* = \frac{I^*}{\rho + \delta}\left(\gamma + \frac{r}{1 + \epsilon I^*}\right)$

and I^* is the positive root of the following equation,

$f(I) = A_3 I^3 + A_2 I^2 + A_1 I + A_0 = 0$

where

$A_0 = \frac{\alpha}{K\beta^2}(\rho + \gamma + r)^2 \left(1 - \frac{K\beta}{\rho+\gamma+r}\right)$,

$A_1 = \rho\left(1 + \frac{\gamma}{\rho+\delta} + \frac{r}{\rho+\delta}\right) + \frac{2\alpha\epsilon\,(\rho+\gamma)}{K\beta^2}(\rho+\gamma+r) - \frac{\alpha\epsilon}{\beta}(2\rho + 2\gamma + r)$,

$A_2 = 2\rho\,\epsilon + \frac{\rho\,\epsilon}{\rho+\delta}(2\gamma + r) + \frac{\alpha}{K\,\beta^2}(\rho+\gamma)^2\,\epsilon^2\left(1 - \frac{K\beta}{\rho+\gamma}\right)$,

$A_3 = \left(\rho + \frac{\rho\,\gamma}{\rho+\delta}\right)\epsilon^2$.

It is evident that the coefficient A_3 is always positive. Additionally, we observe that $A_0 > 0$ when $R_0 < 1$, and $A_0 < 0$ when $R_0 > 1$. The discriminant D of the cubic polynomial f is expressed as

$D = A_1^2 A_2^2 - 4 A_0 A_2^3 - 4 A_1^3 A_3 + 18 A_0 A_1 A_2 A_3 - 27 A_0^2 A_3^2$. $\qquad$ (5)

This discriminant characterizes the nature of the roots of the polynomial: if $D < 0$, the polynomial has one real root and a pair of complex conjugate roots; if $D = 0$, it has three real roots, at least two of which coincide; and if $D > 0$, all three roots are real and distinct. Let x_1 and x_2 denote the critical points of f, defined as the solutions of its first derivative. These points are given by:

$x_{1,2} = \frac{-2A_2 \pm \sqrt{4A_2^2 - 12A_1 A_2}}{6A_3}$.

Now, we regard the case when $R_0 < 1$. In this scenario, we have $f(0) = A_0 > 0$. If x_1 is a complex number or $x_1 \leq 0$, the function f is monotonically increasing on the interval $(0, \infty)$, implying that it possesses no positive real roots. This observation facilitates a graphical interpretation of the root structure, leading to the formulation of the following theorem.

Theorem 1. Assume $R_0 < 1$ and D is given by (5).

- If $D < 0$, the system (1)-(3) does not admit any endemic equilibria.
- If $D = 0$, there exists a unique endemic equilibrium provided that $x_1 > 0$; otherwise, no endemic equilibria exist.

- If $D > 0$, the system (1)-(3) has two endemic equilibria when $x_1 > 0$, and no endemic equilibria if this condition is not met.

Now, consider the case when $R_0 > 1$, which implies that $f(0) = A_0 < 0$. In this setting, if the critical point x_2 is either complex or satisfies $x_2 \geq 0$, the function f is strictly increasing on the interval $(-\infty, 0)$. As a result, the polynomial has no negative real roots. Based on this behavior, we are able to establish the following theorem.

Theorem 2. Assume $R_0 > 1$. Then the system (1)-(3) has a unique endemic equilibrium.

Theorem 3. Assume $R_0 = 1$.

- If $A_1 < 0$, then the system (1)-(3) has a unique endemic equilibrium.
- If $A_1 \geq 0$ and $A_2 \geq 0$, then the system (1)-(3) has no endemic equilibria.

The Jacobian matrix corresponding to the model (1)-(3) as follows:

$$
J = \begin{bmatrix}
\alpha - \dfrac{2\alpha S}{K} - \beta I & -\beta S & \delta \\
\beta I & \beta S - \rho - \gamma - \dfrac{r}{(1 + \epsilon I)^2} & 0 \\
0 & \gamma + \dfrac{r}{(1 + \epsilon I)^2} & -(\rho + \delta)
\end{bmatrix}.
$$

Theorem 4. The disease free equilibrium E^0 of the system (1)-(3) is locally asymptotically stable when $R_0 < 1$, and becomes unstable when $R_0 > 1$.

Proof. The Jacobian matrix corresponding to $E^0 = (K, 0, 0)$ of model (1)-(3) is as follows:

$$
J^0 = \begin{bmatrix}
-\alpha & -\beta K & \delta \\
\beta I & \beta K - (\rho + \gamma + r) & 0 \\
0 & \delta + r & -(\rho + \delta)
\end{bmatrix}.
$$

The eigenvalues of J^0 are

- $\lambda_1 = -\alpha$,
- $\lambda_2 = -(\rho + \delta)$,
- $\lambda_3 = (\rho + \gamma + r)(R_0 - 1)$.

It is clear that $\lambda_1, \lambda_2 < 0$. Note that if $R_0 < 1$, $\lambda_3 < 0$ and so the disease-free equilibrium E^0 is locally asymptotically stable. Conversely, if $R_0 > 1$, $\lambda_3 > 0$ and so E^0 is unstable.

Theorem 5. If $R_0 > 1$ then the system (1)-(3) has a unique infected equilibrium E^* and in this instance E^* locally asymptotically stable provided the following condition is satisfied

- $B_1 B_2 > B_3$,

where

- $B_1 = \frac{2\alpha S^*}{K} - \alpha + \beta I^* - \beta S^* + 2\rho + \gamma + \delta$,
- $B_2 = \left(\alpha - \frac{2\alpha S^*}{K} - \beta I^*\right)\left(\beta S^* - \rho - \gamma - \frac{r}{(1+\epsilon I^*)^2}\right)$

    $+(\rho + \delta)\left(-\alpha + \frac{2\alpha S^*}{K} + \beta I^* - \beta S^* + \rho + \gamma + \frac{r}{(1+\epsilon I^*)^2}\right) + \beta^2 S^* I^*$,

- $B_3 = (\rho + \delta)\left(\alpha - \frac{2\alpha S^*}{K} - \beta I^*\right)\left(\beta S^* - \rho - \gamma - \frac{r}{(1+\epsilon I^*)^2}\right)$

    $+(\rho + \delta)\beta^2 I^* S^* - \gamma \delta \beta I^* - \frac{r \beta \delta}{(1+\epsilon I^*)^2}$.

Proof. The Jacobian matrix corresponding to $E^* = (S^*, I^*, R^*)$ of the system (1)-(3) is as follows:

$$J^* = \begin{bmatrix} \alpha - \dfrac{2\alpha S^*}{K} - \beta I^* & -\beta S^* & \delta \\ \beta I^* & \beta S^* - \rho - \gamma - \dfrac{r}{(1+\epsilon I^*)^2} & 0 \\ 0 & \gamma + \dfrac{r}{(1+\epsilon I^*)^2} & -(\rho + \delta) \end{bmatrix}$$

and the characteristic equation is $\lambda^3 + B_1 \lambda^2 + B_2 \lambda + B_3 = 0$.

If $B_1 B_2 > B_3$ then by Routh-Hurwitz criterion, characteristic equation of J^* as the roots which are negative or with negative real parts. Therefore, we finalize that E^* is locally asymptotically stable for $R_0 > 1$ supplied $B_1 B_2 > B_3$.

Hopf Bifurcation and Numerical Example

In this section, we concentrate on the case where $R_0 > 1$ and examine the Hopf bifurcation occurring around the positive equilibrium $E^* = (S^*, I^*, R^*)$.

Theorem 6. Let $R_0 > 1$.

- If the inequality $B_1 B_2 > B_3$ holds, then the positive equilibrium E^* of the system (1)-(3) is conditionally stable.
- Conversely, if $B_1 B_2 < B_3$, this leads the system (1)–(3) to experience a Hopf bifurcation at E^*.

Next, we demonstrate the occurrence of a Hopf bifurcation for the system (1)–(3) through a numerical example.

Example 1. Firstly, we take $\alpha = 0.5, K = 50, \delta = 0.001, \beta = 0.05, \rho = 0.2, \gamma = 0.1, r = 0.5, \epsilon = 5$. In this case $R_0 > 1$ and the system (1)-(3) has a unique endemic equilibrium. Figure 1 and Figure 2 show that E^* is locally asimptotically stable when $B_1 B_2 > B_3$. Later, we take $\alpha = 0.5, K = 100, \delta = 0.001, \beta = 0.5, \rho = 0.8, \gamma = 0.1, r = 0.8, \epsilon = 1$, and we observe that E^* loses its stability, leading to the occurrence of a Hopf bifurcation, where a family of periodic solutions emerges from E^* when $B_1 B_2 < B_3$ (see Figure 3 and Figure 4).
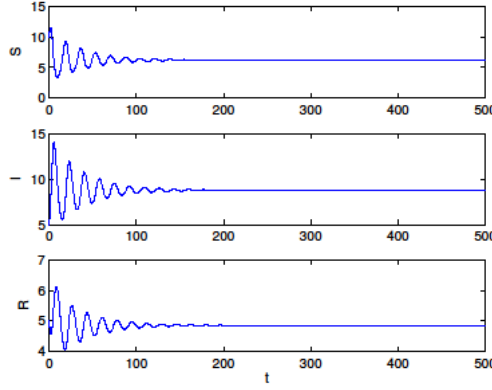
Figure 1. When $B_1 B_2 > B_3$, E^* is asiymptotically stable.
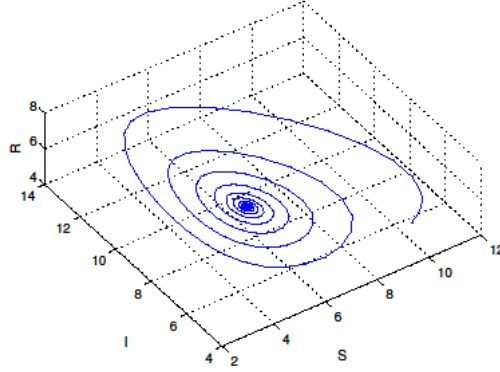
Figure 2. Phase portrait of E^* when $B_1 B_2 > B_3$.

It can be observed from Figures 1 and 2 that the system converges to the endemic equilibrium E^*, confirming its asymptotic stability.
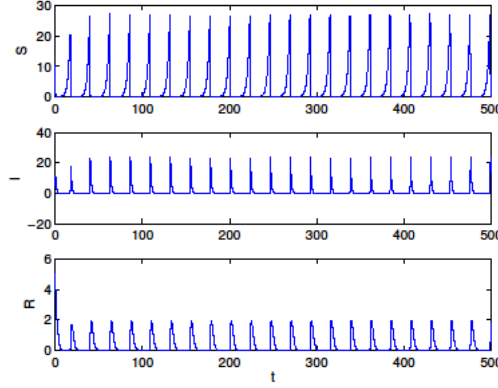
Figure 3. When $B_1 B_2 < B_3$, E^* demonstrates Hopf bifurcation.
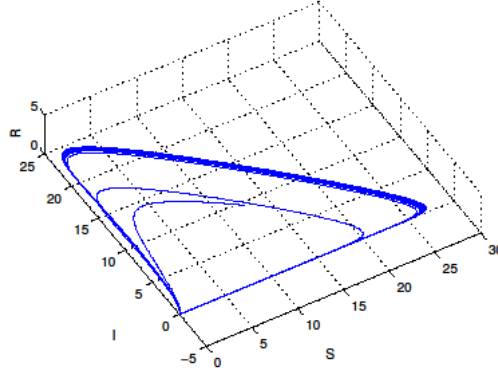
Figure 4. Phase portrait of E^* when $B_1 B_2 < B_3$.

Figures 3 and 4 clearly demonstrate the emergence of limit cycle oscillations, confirming the occurrence of Hopf bifurcation predicted theoretically.

RESULTS AND DISCUSSION

In this section, we present and analyze the primary analytical and numerical findings for the proposed SIRS epidemic model incorporating logistic growth and saturated treatment. Initially, we examined the local stability of both the disease-free and endemic equilibria. Our results indicate that the disease-free equilibrium is locally asymptotically stable for values of the basic reproduction number $R_0 < 1$, whereas it becomes unstable once R_0 exceeds unity. This threshold behavior is consistent with classical epidemic theory, suggesting that the disease can be controlled and potentially eliminated if interventions successfully reduce R_0 below one. Additionally, we explored the conditions for the occurrence of Hopf bifurcation at the

endemic equilibrium. Utilizing Hopf bifurcation theory alongside the Routh–Hurwitz criteria, we established sufficient conditions that guarantee the system undergoes a Hopf bifurcation, leading to oscillatory dynamics around the endemic state. These conditions reveal that the nonlinear saturation in treatment, combined with logistic population growth, can lead to oscillatory behavior in disease prevalence.

To validate the theoretical results, we performed computational experiments using MATLAB. The simulations confirm the analytical findings: when the system parameters are such that $R_0 < 1$, the infection dies out over time. However, for $R_0 > 1$ and under certain parameter ranges satisfying the Hopf bifurcation criteria, the system exhibits sustained oscillations around the endemic equilibrium. This behavior highlights the complex dynamics that can arise from the interaction between saturation in treatment capacity and limited population growth.

These findings underline the importance of considering treatment saturation in epidemiological models. In real-world scenarios, medical resources are often limited, and such saturation effects can significantly influence the long-term behavior of disease dynamics. Our results suggest that increasing treatment capacity or improving efficiency can prevent the onset of oscillatory outbreaks and promote disease control.

In summary, the model exhibits rich dynamical behavior depending on key parameters, and the occurrence of Hopf bifurcation provides important insights into the conditions under which recurrent outbreaks may arise. This emphasizes the necessity of carefully managing treatment resources in public health planning.

REFERENCE

Bhowmick, S., Sokolov, I. M., & Lentz, H. H. K. (2022). Decoding the double trouble: A mathematical modelling of co-infection dynamics of SARS-CoV-2 and influenza-like illness, arXiv preprint arXiv:2210.05649.

El Khalifi, M., & Britton, T. (2022). Extending SIRS epidemics to allow for gradual waning of immunity, arXiv preprint arXiv:2211.09062.

Kusbeyzi Aybar, I. (2019). A dynamical analysis of the virus replication epidemic model. TWMS Journal of Applied and Engineering Mathematics, 9(2), 206–219.

Li, J., Teng, Z., Wang, G., Zhang, L., and Hu, C. (2017). Stability and bifurcation analysis of an SIR epidemic model with logistic growth and saturated treatment. Chaos, Solitons & Fractals, 99, 63–70.

Nesteruk, I. (2024). General SIR model for visible and hidden epidemic dynamics, medRxiv.

Pérez, Á. G. C., Vales, E. A., and Almeida, G. E. G. (2019). Bifurcation analysis of an SIR model with logistic growth, nonlinear incidence, and saturated treatment. Complexity, 21 pages.

Tian, X., Xu, R., Bai, N., and Lin, J. (2020). Bifurcation analysis of an age-structured SIRI epidemic model. Mathematical Biosciences and Engineering, 17(6), 7130–7150.

Zafarnejad, R., Griffin, P. M., & Ventresca, M. (2022). A joint compartmental model for the co-infection of SARS-CoV-2 and influenza. medRxiv.

Hybrid Supercapacitor Electrode Materials

Murat ATES[1]

1- Prof. Dr..; Tekirdağ Namık Kemal Üniversitesi, Fen-Edebiyat Fakültesi, Kimya Bölümü. mates@nku.edu.tr, ORCID No: 0000-0002-1806-0330

ABSTRACT

In this study, supercapacitors (SCs) are used as energy storage systems that divided into 3 main sections. These are electrical double layer capacitance (EDLC), pseudocapacitance (PC) and hybrid capacitors (HCs). We have focused on especially on hybrid supercapacitors electrode materials. Carboneous materials have EDLC mechanism. However, metal oxides and conducting polymers show PC mechanism. PC mechanisms have redox reactions in fast electron transfer. Moreover, HC has both EDLC and PC systems. Therefore, HC materials include the combination of these materials. In addiition, SC components are very important to obtain higher electrochemical performances, such as electrolyte type, electrode material, mambrane, used voltage, used methods, etc. Aqueous electrolytes mostly supply good ionic diffusion and conductivity, which enhance the electrochemical performance of SC device.

Keywords – Supercapacitors, EDLC, power density, graphene, pseudocapacitance

INTRODUCTION

Supercapacitors (SCs) have higher electrochemical performances than the other energy storage systems (Li and Xie, 2012:106). There are many various electrode materials for supercapacitors because of their better ion transfer capability and cycle life (Jiang et al., 2020:199).
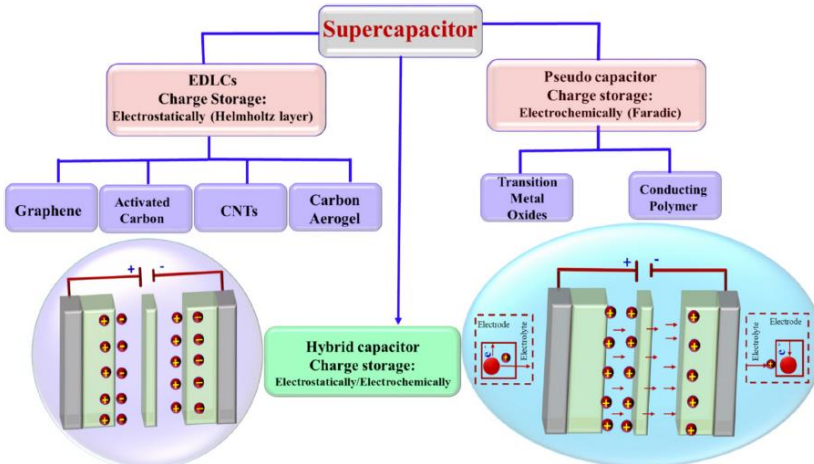

Figure 1: Classification of supercapacitor (Nagarajarao et al., 2022:5; Ansari et al., 2025:115564).

Nowdays, supercapacitors are used together with solar panel systems to collect sunlight using photo-voltaic cells (Viswanathan and Sheety, 2018).

Electric double layer capacitance (EDLC)

EDLC system shows ion movement in Helmoltz plane. However, PC mechanism occurs with oxidation-reduction reactions on the electrode surface (Saha et al., 2016; Liao et al., 2018:3861).

Graphene oxide (GO) is obtained from graphite using oxidizers such as $KMnO_4$ by Hummers method. It has a single layer of materials and good dispersion of water because of its functional groups (Sharma and Lee., 2016:563; Chen et al., 2012:6027). Graphene is a 2D nanosheets, which mostly used in SCs. It is a graphitic nanosheet with a few atom thicks. Therefore, it supplies good mechanical and thermal behaviors. Moreover, it can be used in the component of electrode materials. It is also used in different fields, such as solar cells, chemical detectors, batteries and supercapacitors (Sykes, 2009:175).
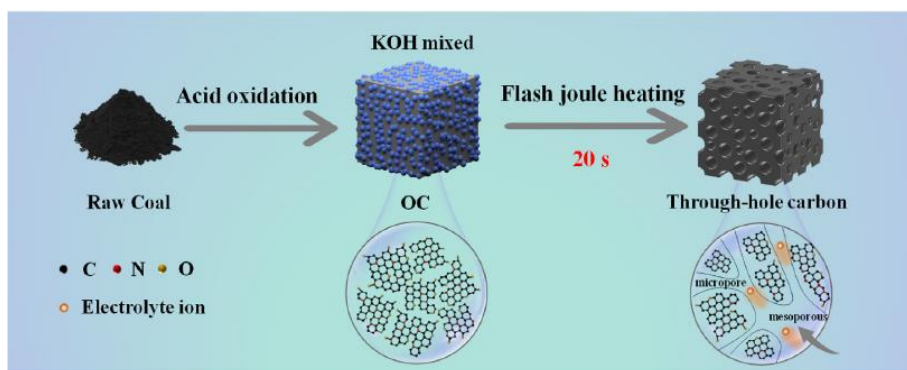
Figure 2: Formation of active carbon using FJH method (Gao et al., 2025:237129).

In literature, graphene has a high surface area of ~2600 m^2/g (Ivanosckii, 2012:571) and good specific capacitance of C_{sp}=550 F/g (Chen et al., 2013).

Active carbon synthesis using FJH method show that functional groups display significant role on conductivity and wettability of supercapacitors, which have significant to the performance of supercapacitors (Cai et al., 2023:118368). **Pore size** is very critical importance for AC materials. The micropores (<2 nm) show a larger surface area and provide more active sites for supercapacitors. Ultra-micropore (< 0.7 nm) can mostly reduce the thickness of the EDLC. Thus, it improves the electrochemical performance of supercapacitors. Moreover, meso-pores (between 2 and 50 nm) supply ion movements. Moreover, large pores (>50 nm) are called macropores, which are conductive to electrolyte storage (Su et al., 2017:73).

Pesudocapacitace (PC)

In literature, **conducting polymers** are used as a most potential electrode material component due to its good electrical conductivity, facile synthesis, cheaper and high energy storage capability (Sun and Chen, 2009:924). Conducting polymers supply an electrical conductivity due to their π-conjugation structures (Shulga et al., 2014). As a result, they enable the high electrochemical performances of SCs. Although they also show doed and undoped process in their chemical skeleton, they have low charge-discharge stability.

Polythiophenes (PThs) are used in different area, such as batteries (Ansari et al., 2025:115564), electrochromic devices (Srivastava, et al., 2025:889), electrochemical sensors (Shahzad and Afzal, 2025:163) and supercapacitors, etc. (Xiao et al., 2025:09673911241304848).

Polyaniline (PANI) is mostly used in SCs due to its facile synthesis, eco-friendly, cheaper and recersible electrochemical redox states (Solonaru and Grigoras, 2017:127).

Moreover, transition metal oxides supply redox reactions due to their more oxidation states. They have limited electrochemical performances. In addition, their charge-discharge stability is very low because of the development of cracks in the active materials (Zhi et al., 2013).

Ruthenium oxide (RuO_2) is very expensive metal oxide compared to other metal oxides, such as NiO, CuO, Fe_2O_3, V_2O_5, Co_2O_3, etc. (Xiong et al., 2014). It shows good electrochemical performances for SCs due to changeable oxidation states and good electrical conductivity (Cho et al., 2015). Titanium dioxide (TiO_2) is mostly used in semiconductor technology due to good electronic properties, physical and chamical stability and low-cost (Phan et al., 2016).

Hybrid Supercapacitors (HC)

Polypyrrole (PPy) nanowires and GO nanosheets are synthesized by in-situ polymerization inside GO suspension solution and pyrrole monomer. The specific capacitance of GO/PPy electrode was presented as C_{sp}= 633 F/g at 1 A/g.

Figure 3: Synthesis illustration of GO/Th/PEDOT electrode (Wang, et al., 2015:370; Ansari et al., 2025;115564).

In literature, graphene/TiO_2 nanocomposites were presented using different methods (Meng et.al., 2011:165602; Zhang et al., 2011:274). Moreover, graphene/Co_3O_4 electrode was given with a good electrochemical performances of C_{sp}=392 F/g at 1 A/g (Wang et al., 2017:1750102).
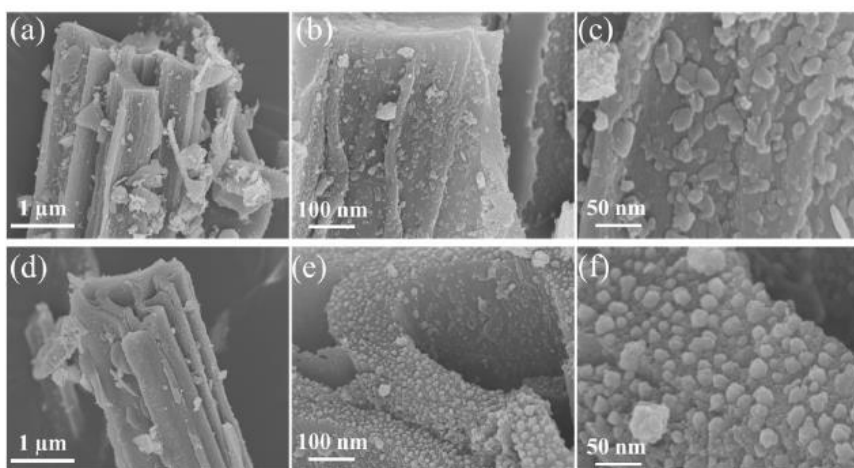

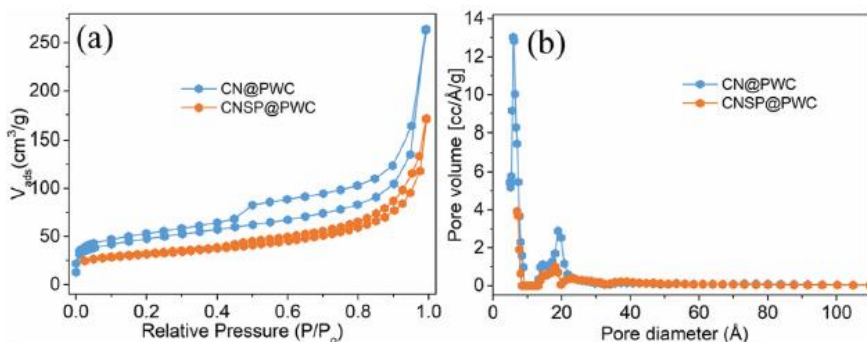Figure 4: SEM images of the (a, b, c) CN@PWC and (d, e, f) CNSP@PWC nanocomposites (Prabu et al., 2025:236705).

Figure 5: BET plots a) CN@PWC and CNSP@PWC materials and b) pore size distribution (Prabu et al., 2025:236705).

In literature, $CoNi_3S_4$ (P)@pine wood-derived carbon (PWC) electrode (CNSP@PWC) were presented as a dood electrochemical performances (801 C/g at 0.5 A/g) in 1 M KOH and Na_2SO_4 electrolyte solution. Their FE-SEM and BET analysis images were given in **Figure 4 and 5**. It has a good capacity protection (90% at 10 A/g for 5000 charge-discharge cycles) (Prabu et al., 2025:236705). In addition, MnO_2/carbon fiber electrores showed a good specific capacitance of C_{sp}=151.1 F/g (Ning et al., 2016:754).

Synthesis methods and used parameters

There are many synthesis methods for fabrication of electrode materials. These are chemical oxidation (Alvi et al., 2011:9406), electrochemical deposition (Lee et al., 2012:1899), vapor phase polymerization (Chen et al., 2013:1152), etc.

The pH is also another parameter to achieve the best efficiency. It should be compatible with the electrode material. For example, PPy/graphene electrodes were studied in 3 different solutin medium. The highest specific capacitance was measured as C_{sp}= 646.5 F/g at 10 mV/s in acidic mesium (Cai et al., 2011:460; Haciismailoglu et al., 2024:3315; Sharma et al., 2008:268).

In literature, organic frameworks with triazine (COFs-CTF) were synthesized and showed a good specific capacity of 159.8 mAh/g at 1 A/g (He et al., 2025:116291).
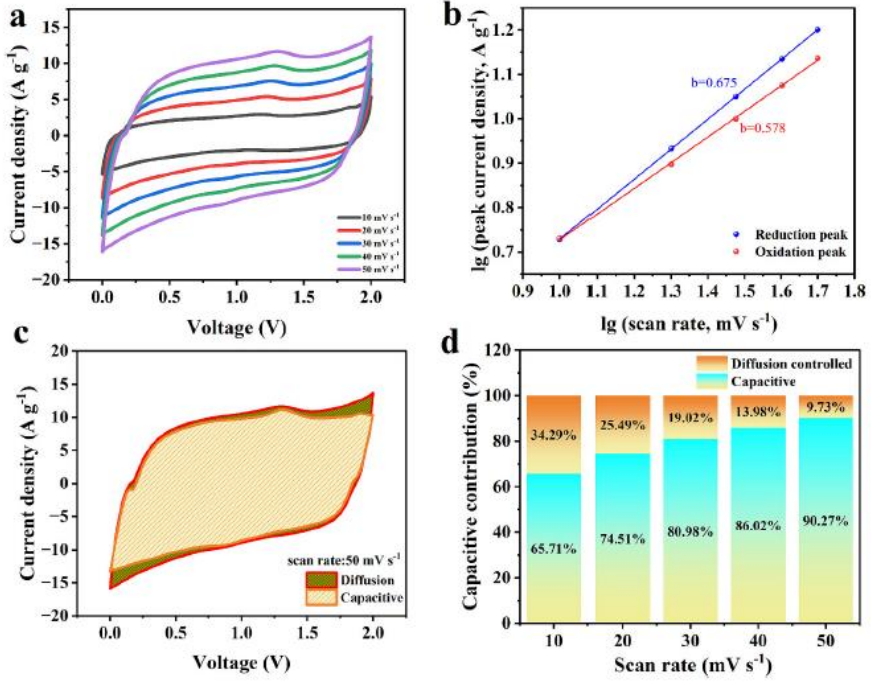
Figure 6: Kinetic plot of ZIC based on AC-CTF-COF-800. a) CV plots at different scan rates, b) The fitting plot between lg(i) and lg(v). c) CV plots with the diffusion contribution at 50 mV/s. d) Diffusion contribution at different scan rates (He et al., 2025:116291).
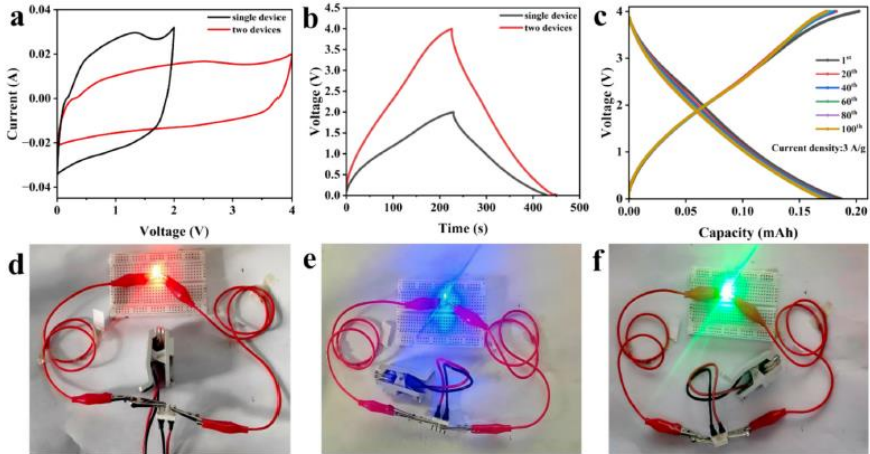

Figure 7: a) CV plots of a single ZIC and two ZICs connected in series at a 100 mV/s, b) GCD plots of a single ZIC and two ZICs connected in series at a current density of 3 A/g, c) GCD plots of two ZICs connected in series for 100 cycles at a current density of 3 A/g, d-f) Photographs of LEDs (red, blue and green) powered by two ZICs conected in series (He et al., 2025:116291).

Inkjet printing can be used with various properties such as shape, dimensions of materials using computer-aided layout and thickness in SCs (Li et al., 2020:144872). It supplies good electrical conductivity and thermal stability (Liu et al., 2016:385603). The printed graphene have many advantages such as high electrical conductivity (26000 S/cm), electron mobility (2×10^5 cm^2/V$\times$s) (Li et al., 2014:19095).

RESULTS AND DISCUSSION

In this study, hybrid supercapacitor electrode materials were investigated 3 main sections (EDLC, PCs and HCs). Carbaneous materials such as graphene oxide (GO), active carbon (AC), etc. were given in more detail. Surface area and pore size effects were presented in carbaneous materials. PCs were given as conducting polymers such as PThs and PANI and transition metal oxides. Some examples were also given especially for HCs from literature. Lastly, synthesis methods and SC components were analyzed to obtain higher electrochemical performances of SCs.

REFERENCE

Ansari, K.B., Mashkoor, R, Naim, M.A., Rahman, A.R.S., Ansari, M.Y., Khan, P., Hasib, R., Shkir, M (2025). A critical review on pure and hybrid electrode supercapacitors, economics of HESCs, and future perspectives, J. Energy Storage, 112, Article number: 115564.

Alvi, F., Ram, M.K., Basnayaka, P.A., Stefanakos, E, Goswami, Y., Kumar, A. (2011) Graphene-polyethylenedioxythiophene conducting polymer composite based supercapacitor. Electrochim. Acta, 56, 9406-9412.

Cai, M., Wei, X., Huang, H., Yuan, F., Li, C., Xu, S., Liang, X., Zhou, W., Guo, J. (2023). Nitrogen doped Ti$_3$C$_2$T$_x$ MXene prepared by thermal decomposition of ammonium salts and its application in flexible quasi-solid state supercapacitors. Chem. Eng. J., 458, Article number: 118368.

Cai, Y., Qin, Z., Chen, L. (2011). Effect of electrolytes on electrochemical properties of graphene sheet covered with polypyrrole thin layer. Prog. Nat. Sci. Mater., 21(6), 460-466.

Chen, D., Feng, H., Li, J (2012). Graphene oxide: preparation, functionalization, and electrochemical applications. Chem. Rev., 112, 6027-6053.

Chen, J., Li, C., Shi, G. (2013). Graphene materials for electrochemical capacitors. J. Phys. Chem. Lett., 4, 1244-1253.

Chen, Y., Xu, J., Mao, Y., Yang, Y., Yang, W., Li, S. (2013). Electrochemical performance of graphene-polyethylenedioxythiophene nanocomposites. Mater. Sci. Eng. B, 178, 1152-1157.

Cho, S., Kim, M., Jang, J. (2015). Screen-printable and flexible RuO$_2$ nanoparticle decorated PEDOT:PSS / graphene nanocomposite with enhanced electrical and electrochemical performances for high-capacity supercapacitor, ACS Appl. Mater. Interfaces, 7, 10213-10227.

Gao, H., Li, Y., Wu, X., Lv, Y., Ma, C., Pei, Y., Liang, N., Meng, F., Dong, P., Guo, J. (2025). Ultrafast activation to form through-hole carbon facilities ion transport for high specific capacity supercapacitors. J. Power Sources, 644, Article number: 237129.

Haciismailoglu, M., Vatansever, D., Alper, M. (2024). Polypyrrole-oxalate and polypyrrole-sulfate electrodes for supercapacitor applications. Chem. Pap., 78, 3315-3329.

He, J., Yang, S., Guo, Y., Mi, Y., Du, P. (2025). Porous carbon materials derived from triazine structured COFs for high-performance zinc-ion supercapacitors. J. Energy Storage, 118, Article number: 116291.

Inavovskii, A.L. (2012). Graphene-based and graphene-like materials. Russian Chemical Reviews, 81, 571-605.

Jiang, F.T., Fang, Y.Z., Xue, Q.S., Chen, L., Lu, Y. (2010). Graphene based carbon nano-fibers grown on thin sheet sinter-locked Ni-fiber as self-supported electrodes for supercapacitors. Mater. Lett., 64, 199-202.

Lee, S., Cho, M.S., Lee, H., Nam, J.D., Lee, Y. (2012). A facile synthetic route for well-defined multilayer films of graphene and PEDOT via on electrochemical method. J. Mater. Chem., 22, 1899-1903.

Li, J., Xie, H. (2012). Synthesis of graphene oxide / polypyrrole nanowire composites for supercapacitors. Mater. Letters, 78, 106-109.

Li, L., Guo, Y., Zhang, X., Song, Y. (2014). Inkjet-printed highly conductive transparent patterns with water based Ag-doped graphene. J. Mater. Chem. A., 2, 19095-19101.

Li, X., Zhao, J., Yu, J., Liu, Q., Chen, R., Zhang, H., Song, D., Liu, J., Wang, J. (2020). Layer by layer inkjet printing reduced graphene oxide film supported nickel cobalt layered double hydroxide as a binder free electrode for supercapacitors. Appl.Surf. Sci., 509, Article number: 144872.

Liao, C.Y., Chien, H.H., Hao, Y.C., Chen, C.W., Yu, I.S., Chen, J.Z. (2018). Low temperature-annealed reduced graphene oxide-polyaniline nanocomposites for supercapacitor applications, Journal of Electronic Materials, 47(7), 3861-3868.

Liu, P., Ma, J., Deng, S., Zeng, K., Deng, D., Xie, W., Lu, A. (2016). Graphene-Ag nanohexagonal platelets-based ink with high electrical properties at low sintering temperatures. Nanotechnology, 27, Article number: 385603.

Meng, X., Geng, D., Liu, J., Li, R., Sun, X. (2011). Controllable synthesis of graphene-based titanium dioxide nanocomposites by atomic layer deposition, Nanotechnology, 22(16), Article number: 165602.

Nagarajarao, S.H., Nandagudi, A., Viswanatha, R., Basavaraja, B.M., Santesh, M.S., Praveen, B.M., Pandith, A. (2022). Recent developments in supercapacitor electrodes: Amini review. ChemEngineering, 6(1), Article number: 5.

Ning, P., Duan, X., Ju, X., Lin, X., Tong, X., Pan, X., Wang, T., Li, Q. (2016). Facile synthesis of carbon nanofibers / MnO_2 nanosheets as high-performance electrodes for asymmetric supercapacitors. Electrochim. Acta, 210, 754-761.

Prabu, S., Chiang, K.Y., Alodhayb, A.N., Pandiaraj, S., Pallavolu, M.R. (2025). Integrated electrode-electrolyte optimization to fabricate pinewood-derived carbon permeated $CoNi_3S_4$ (P) hybrid nanocomposites as redox-rich electrode materials for ultra-high energy density hybrid supercapacitors. J. Power Sources, 640, Article number: 236705.

Phan, T.B., Luong, T.T., Mai, T.X., Mai, T.T.T., Pham, T.T. (2016). Effect of nanostructured graphene oxide on electrochemical activity of its composite with polyaniline titanium dioxide. Adv. Nat. Sci.: Nanosci. Nanotechnol, 7, Article number: 015016.

Sharma, A., Lee, B.K. (2016). Integrated ternary nanocomposite of TiO_2/NiO/reduced graphene oxide as a visible light photocatalyst for efficient degradation of o-chlorophenol. J. Environ. Manag. 181, 563-573.

Su, H., Zhang, H., Liu, F., Chun, F., Zhnag, B., Chu, X., Huang, H., Deng, W., Gu, B., Zhnag, H., Zheng, X., Zhu, M., Yang, W. (2017). High power supercapacitors based on hierarchically porous sheet-like nanocarbons with ionic liquid electrolytes. Chem. Eng. J., 322, 73-81.

Saha, S., Chhetri, S., Khanna, P., Samanta, P., Koo, H., Murmu, N.C., Kuila, T. (2016). In-situ hydrothermal synthesis of MnO_2/NiO@Ni heterostructure electrode for hydrogen evolution reaction and high energy asymmetric supercapacitor applications. J. Energy Storage, 6, 22-31.

Shahzad, N., Afzal, A. (2025). Molecularly imprinted nanocomposites-based synthetic antibodies for uric acid-specific non-invasive electrochemical gut sensors, Microchimica Acta, 192(3), Article number: 163.

Sharma, R.K., Rastogi, A.C., Desu, S.B. (2008). Pulse polymerized polypyrrole electrodes for high energy density electrochemical supercapacitor. Electrochem. Commun., 10, 268-272.

Sykes, E.C. (2009). Surface assembly-graphene goes underwater, Nat. Chem., 1(3), 175-176.

Srivastava, S., Sahu, B., Mishra, D., Bansal, L., Ahlawat, N., Rath, DK, Rout, P.S., Kumar, S., Singh, S., Pandey, S. (2025). Polymer-MXene-viologen-based suprahybrid electrochromic device: Flexible smart window with visible and near-infrared switchability, ACS Appl. Optical Mater., 3(4), 889-897.

Solonaru, A.M., Grigoras, M. (2017). Water soluble polyaniline/graphene composites as materials for energy storage applications. Express Polymer Letters, 11(2), 127-139.

Sun, W., Chen, X.Y. (2009). Preparation and characterization of polypyrrole films for three-dimensional micro-supercapacitor. J. Power Sources, 193, 924-929.

Shulga, Y.M., Baskakov, S.A., Samirnov, V.A., Shulga, N.Y., Brlay, K.G., Gutsev, G.L. (2014). Graphene oxide films as separators of polyaniline-based supercapacitors. J. Power Sources, 245, 33-36.

Viswanathan, A., Sheety, A.N. (2018). Single step synthesis of rGO, copper oxide and polyaniline nanocomposites for high energy supercapacitors, Electrochim. Acta, 289, 204-217.

Wang, Y., Ma, R., Liu, L. (2017). A facile one pot method for Co_3O_4/graphene composite as efficient electrode materials for supercapacitors. Nano Brief Reports and Reviews, 12(8), Article number: 1750102.

Wang, M., Jamal, R., Wang, Y., Yang, L., Liu, F., Abdiryim, T. (2015). Functionalization of graphene oxide and its composite with poly(3,4-ethylenedioxythiophene) as electrode material for supercapacitors. Nanoscale Res. Lett., 10, Article number: 370.

Xiao, D.Q., Sun, B., Liu, Y.B., Jiao, E.X., Wang, X., Chen, X.M., Cheng, X.F., Guo, K., Yuan, K.S., Zhang, H.J. (2025). Development status of supercapacitors and their widely applied organic semi-conductors:

Polythiophene conjugated polymers, Polymers & Polymer Composites, 33, Article number: 09673911241304848.

Xiong, P., Huang, H., Wang, X. (2014). Design and synthesis of ternary cobalt ferrite / graphene / polyaniline hierarchical nanocomposites for high-performance supercapacitors. J. Power Sources, 245, 937-946.

Zhi, M., Xiang, C., Li, J., Li, M., Wu, N. (2013). Nanostructured carbon-metal oxide composite electrodes for supercapacitors: a review, Nanoscale, 5, 72-88.

Zhang, H., Xu, P., Du, G.D., Chen, Z.W., Oh, K., Pan, D.Y., Jiao, Z. (2011). A facile one-step synthesis of TiO_2/graphene composites for photo-degradation of methyl orange, Nano Res., 4(3), 274-283.